INL/EXT-11-21436

Final Report on Utilization of TRU TRISO Fuel as Applied to HTR Systems Part I: Pebble Bed Reactors

B. Boer
A. M. Ougouag

March 2011

The INL is a U.S. Department of Energy National Laboratory
operated by Battelle Energy Alliance

INL/EXT-11-21436
FCRD-FUEL-2011-000062

Final Report on Utilization of TRU TRISO Fuel as Applied to HTR Systems Part I: Pebble Bed Reactors

B. Boer
A. M. Ougouag

March 2011

Idaho National Laboratory
Fuel Cycle Research & Development
Idaho Falls, Idaho 83415

http://www.inl.gov

Prepared for the
U.S. Department of Energy
Office of Nuclear Energy
Under DOE Idaho Operations Office
Contract DE-AC07-05ID14517

Author:

A. M. Ougouag 03/29/2011
For Brian Boer Date
A. M. OUGOUAG

Reviewed by:

3/29/2011
Michael A. Pope Date

Concurred by:

A. M. Ougouag 03/29/2011
Co-Author and Work Package Manager Abderrafi M. Ougouag Date

SUMMARY

The deep burn (DB) project aims at the destruction of legacy inventories of plutonium (Pu) and minor actinides (ma) leftover in used fuel from the operation of light water reactors (LWR). In its initial phase, the project examined the performance of high temperature reactors (HTR) for the db purpose. The performance is assessed based on two principal criteria. The first of these is "effectiveness," which pertains to the ability of the concept to indeed result in significant reduction of the Pu and MA inventories. The second criterion is "safety," which, for TRISO-based fuel, pertains primarily to the continuity of integrity of the TRISO particle, the primary barrier to the release of radionuclides from the fuel to the near field (i.e., within the reactor plant) and beyond (possibly to unrestricted public areas). Most of these issues have been addressed in previous reports. The focus of this final report is to present results on the optimization of the core of a db pebble bed reactor (PBR) and to examine the performance of the fuel in the variant of db that considers features akin to the modified open fuel cycle (MOFC) concept. In the context of this study, MOFC is represented by its implication of the inclusion of selected fission product isotopes and of some americium (am) content into the db fuel.

The most significant accomplishments documented in this report are:

- Core analysis of a HTR-MODULE-type* design loaded with Deep-Burn fuel.
- Core analysis of a HTR-MODULE-type design loaded with Deep-Burn fuel and Uranium.
- Core analysis of a HTR-MODULE-type design loaded with Deep-Burn fuel and Modified Open Cycle Components.
- Core analysis of a HTR-MODULE-type design loaded with Deep-Burn fuel and Americium targets.

A companion report, "Final Report on Utilization of TRU TRISO Fuel as Applied to HTR Systems Part II: Prismatic Reactor Cross Section Generation," addresses cross section preparation for prismatic-block HTRs for application to the Deep Burn concept.

* The HTR-MODULE was a German design of a 200 MWth passively safety pebble bed reactor.

CONTENTS

FIGURES

TABLES

ACRONYMS

BAF	Bacon Anisotropy Factor
BONAMI	Bondarenko method
CB	core barrel
DB	Deep-Burn
DLOFC	depressurized loss of forced cooling
DOE	Department of Energy
EDN	Effective DIDO Nickel (unit of fluence based on nickel activation, converts to E > 0.1 MeV fluence by multiplying by 3.0/1.7)
FIMA	fissions per initial metal atom
FTC	fuel temperature coefficient
IHM	initial heavy metal
INL	Idaho National Laboratory
IPyC	inner pyrolytic carbon
LOFC	Loss of Forced Cooling
LWR	light water reactor
MTC	moderator temperature coefficient
NEA	Nuclear Energy Agency
OECD	Organization for Economic Co-operation and Development
OPyC	outer pyrolytic carbon
PBMR	Pebble Bed Modular Reactor
PBR	pebble bed reactor
RHRS	reactor heat removal system
RPV	reactor pressure vessel
SiC	silicon carbide
TRISO	tri-isotopic
TRU	transuranic
UTC	uniform temperature coefficient

High Temperature Reactor (HTR) Deep Burn Core and Fuel Analysis

Modified Open Cycle component and Am targets

1. INTRODUCTION

The Deep-Burn (DB) concept [1] focuses on the destruction of transuranic nuclides from used light water reactor (LWR) fuel. These transuranic nuclides are incorporated into tri-isotopic (TRISO) coated fuel particles and used in gas-cooled reactors with the aim of a fractional fuel burnup of 60 to 70% in fissions per initial metal atom (FIMA). This high performance is expected through the use of multiple recirculation passes of the fuel in pebble form without any physical or chemical changes between passes. In particular, the concept does not call for reprocessing of the fuel between passes. In principle, the DB pebble bed concept employs the same reactor designs as the presently envisioned low-enriched uranium core designs, such as the 400 MW_{th} Pebble Bed Modular Reactor (PBMR-400) [2].

It has been shown in the previous Fiscal Year* (FY) (2009) that a fully-PuO_2 fueled pebble bed reactor concept is viable. However, achieving a high fuel burnup while remaining within safety-imposed prescribed operational limits for fuel temperature, power peaking, and temperature reactivity feedback coefficients for the entire temperature range, is challenging. The presence of the isotopes ^{239}Pu, ^{240}Pu, and ^{241}Pu that have resonances in the thermal energy range significantly modifies the neutron thermal energy spectrum as compared to a standard, UO_2-fueled core. Therefore, the DB pebble bed core exhibits a relatively hard neutron energy spectrum. However, regions within the pebble bed but near the graphite reflectors experience a locally softer spectrum. This can lead to power and temperature peaking in these regions. Furthermore, a shift of the thermal energy spectrum with increasing temperature can lead to increased neutron interaction in the low-lying fission resonances of the fissile Pu isotopes. This can lead to a positive temperature reactivity coefficient for the graphite moderator under certain operating conditions.

Regarding the coated particle performance, the FY 2009 investigations showed that no significant failure is to be expected for the reference fuel particle during normal operation. It was found, however, that the sensitivity of the stress of the coating to the CO production in the kernel is large. The CO production is expected to be higher in DB fuel than in UO_2 fuel, but its exact level has a high uncertainty. Furthermore, in the fuel performance analysis transient conditions were not yet taken into account.

The effort of this task in FY 2010 has focused on the optimization of the core to maximize the pebble discharge burnup level, while retaining its inherent safety characteristics. Using generic pebble bed reactor cores, this task consists in performing physics calculations to evaluate the capabilities of the pebble bed reactor to perform utilization and destruction of LWR used-fuel transuranics. The task uses established benchmarked models, and introduces modeling advancements appropriate to the nature of the fuel considered (high transuranic [TRU] content and high burn-up).

The following section describes the reference Deep-Burn pebble-bed reactor design in detail. In the section that follows it the goals of the project of Fiscal Year 2010 are restated.

---

* This document is the final report for work that covered FY-2010 and the first trimester of FY-2011, so reference to the previous fiscal year is meant to imply FY-2009

1.1 THE DEEP-BURN PEBBLE-BED REACTOR CONCEPT

The current Deep-Burn Pebble-Bed Reactor design is based on the German HTR-MODULE reactor design [3]. The physical layout of the HTR-MODULE is illustrated in Figure 1, which gives the main characteristics of the reactor. The design features a cylindrical core of slowly downward-flowing pebbles surrounded by graphite reflectors. The mode of operation of the HTR-MODULE is that of (nearly) continuous online reloading and of recirculation of pebbles for multiple passes (typically 15-20) until the target burnup is reached. The pebble-bed core has an average height of 943 cm and a diameter of 300 cm, delivering 200 MW in thermal power.

Although the original design adopted UO_2 fuel the DB version employs Pu-fuel, possibly with Minor Actinides (MA) and irradiation targets (i.e. long-lived fission products). The first studies of a Pu-fueled HTR-MODULE showed the inventory of Pu can be reduced to about one-sixth of the initial [4].

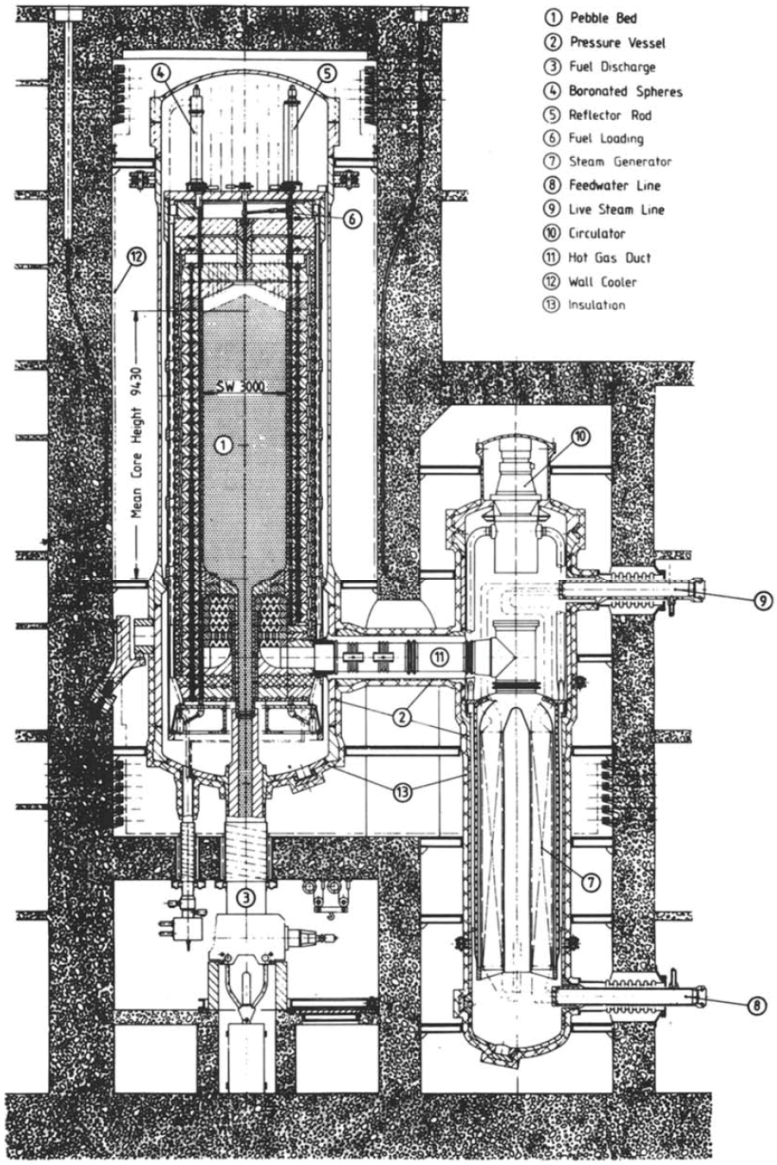

Figure 1. Overview of the HTR-MODULE 200 MW_{th} design [3].

Table 1. Major design and operating characteristics of the HTR-MODULE design.

HTR-MODULE Characteristic	Value
Installed thermal capacity	200 MW(t)
Installed electric capacity	80 MW(e)
Core configuration	Cylindrical pebble-bed (360,000 pebbles)
Pebble bed height	9.43 m
Pebble bed radius	1.50 m
Average power density	3.0 MW/m^3
Fuel	TRISO coated DB-fuel in graphite spheres
Primary coolant	Helium
Primary coolant pressure	6.0 MPa
Mass flow rate	85.6 kg/s
Moderator	Graphite
Core outlet temperature	700°C
Core inlet temperature	275°C

The HTR-MODULE reactor design is very similar to the later HTR-PM design, albeit with differences in power and temperatures. Therefore, understanding the performance of a DB HTR-PM is useful to the present work. Such a study was carried out in the previous fiscal year and complemented more recently. In the previous analyses (see Appendix A-5) of the DB HTR-PM design it was found that for Loss Of Forced Cooling transient conditions the maximum fuel temperature is close to, or exceeds, the generally accepted limit of 1873 K. It is noted that both the average power density (3.0 MW/m^3) and the helium outlet temperature (700 °C) are more modest in the HTR-MODULE than in the HTR-PM design [5], which has an average power density of 3.2 MW/m^3 and a helium outlet of 750 °C. The dimensions of the DB coated particle fuel design are given in Table 2. The composition of the reference DB fuel type considered in the present analysis is shown in Table 3. In principle, both the mix of Pu isotopes from LWR used fuel and some of the neptunium and americium isotopes are used in the DB fuel. The fuel kernel consists of transuranics (TRUs) and a SiC "getter" that reduces the free CO production in the particle (by trapping produced CO). The mole ratio of TRU to SiC, [TRU]:[SiC], in the kernel is 1:0.6, which implies an average density of SiC within the meat of the fuel kernel of 7.6 g/cm^3. The Minor Actinide oxide (MAO_{2-x}) fuel is sub-stoichiometric at 1.8 oxygen atoms per MA atom on average.

Table 2. Dimensions of the coating layers for the DB coated particle design.

Layer	Thickness (μm)
Kernel diameter ($MAO_{1.8}(SiC)_{0.6}$)	350
Buffer	100
IPyC	35
SiC	45
OPyC	35

Table 3. Reference composition of the Deep-Burn fuel considered in the analyses.

Isotope	Fraction (wt. %)
^{237}Np	6.8
^{238}Pu	2.9
^{239}Pu	49.38
^{240}Pu	23
^{241}Pu	8.8
^{242}Pu	4.9
^{241}Am	2.8
^{242m}Am	0.02
^{243}Am	1.4

1.2 TASKS FOR THE DEEP-BURN PEBBLE-BED REACTOR CONCEPT

The main results of the optimization and design activities of the DB pebble bed reactor that have been carried out in FY 2010 are given in the Appendices of this report. The analyses that are presented in the following sections of this report build upon the optimized design that was established in the previous fiscal year. It is found that a cylindrical core design and the use of a diluted fuel particle with an oxygen getter provide a good performance.

1. Investigation of the performance of the DB HTR-MODULE

In the investigations of the previous fiscal year it was found that the cylindrical HTR-PM design performs well in general, but that high fuel temperatures can be encountered in a DLOFC transient for certain conditions. The HTR-MODULE design is similar to the design of the HTR-PM, but has a slightly lower power density (and total reactor power) and is therefore expected to perform better under these adverse conditions. This core design has been analyzed using the PEBBED code for normal conditions as well as for the DLOFC transient.

2. Investigation of the use of a Modified Open Fuel Cycle component

This task is aimed at exploring the performance of the DB-PBR when the fission products of the feed used LWR fuel are not fully removed from the feed and are present in various amounts.

3. Investigation of the use of Americium targets

This task is aimed at exploring the performance of the DB-PBR when dedicated Americium target particles are loaded in the pebbles in combination with the DB fuel particles.

4. Investigation of the use of Uranium in combination with TRU

The addition of Uranium to the DB design is expected to lead to an improvement of the temperature coefficient of reactivity. The effect of the U loading on the temperature coefficient and the achievable discharge burnup are analyzed.

2. OVERVIEW OF THE CODE SYSTEM FOR ANALYSIS OF THE DEEP-BURN PEBBLE-BED REACTOR CORE AND FUEL

In the following two sections, the code systems for analysis of pebble-bed reactor cores and analysis of fuel performance are described, respectively.

2.1 CODE SYSTEM FOR ANALYSIS OF PEBBLE-BED REACTOR CORES

A code-to-code coupling between PEBBED [6] and SCALE-6 [7] has been implemented, which allows PEBBED to read microscopic neutron cross sections in AMPX format as generated with the CSAS5 module of SCALE-6. The fine (238) energy group structure from ENDF/B-VII is collapsed for this purpose to a broad group structure (12 groups, of which 7 are thermal) to be used in PEBBED. Thermal-hydraulic feedback is provided using the THERMIX(-KONVEK) code [8], which is a built-in routine of PEBBED. Short descriptions of the PEBBED code, the cross section generation procedure in SCALE-6, and the THERMIX code are given in the following sections.

2.1.1 DESCRIPTION OF THE PEBBED CODE

The PEBBED code [6] is a tool for analyzing the asymptotic fuel cycle in recirculating pebble bed reactors. Equations for neutron flux and nuclide distribution in a pebble-bed core are solved self-consistently via an iterative scheme. The neutronics solver uses either a standard finite difference technique or a nodal diffusion method. The burnup solver uses a semi-analytical method that guarantees convergence and accuracy. A key step in the algorithm is the computation of the entry plane density of each nuclide of interest in each axial pebble flow channel. These values depend upon the pebble loading and recirculation policy and the burnup accrued by pebbles on successive passes through the core. The current iterate of the flux is used to compute the exit plane nuclide density in a pebble after one pass through the core in each effective channel (corresponding to pebble flow line bundles), based on the density of that nuclide in a fresh pebble. Pebbles are then distributed according to the recirculation scheme to generate the entry plane density in each channel for the subsequent pass. This process is repeated until the pebbles meet or exceed the discharge cutoff burnup. Pebbles that meet of exceed this criterion are removed from further circulation. The retained exit plane values are then averaged according to the recirculation scheme (which may include replacement fresh pebbles) in order to produce the actual entry plane nuclide densities.

2.1.2 CROSS SECTION GENERATION PROCEDURE USING SCALE-6

The Criticality Safety Analysis Sequences (CSAS)(6) module from Standardized Computer Analyses for Licensing Evaluation (SCALE)-6 [7] has been used for the calculation of reactivity coefficients and for the generation of multigroup neutron cross sections to be used in PEBBED. The cross section generation method used here is largely based on a benchmarked SCALE-6 procedure [9]. In this method two lattice cell calculations are performed: (1) a fuel kernel surrounded by coating material and graphite matrix is treated; and (2) a graphite matrix containing TRISO fuel and graphite (which is surrounded by a graphite shell and helium) is used in an infinite lattice calculation. The resonance treatment is performed using the Bondarenko method (BONAMI) for the unresolved resonances range and using CENTRM/PMC/CHOPS for the resolved resonances. CENTRM solves the 1-D transport equation using point wise cross sections to calculate the corresponding point wise spectrum. PMC uses the point wise cross sections, the CENTRM-calculated point wise spectrum, and the multigroup data (where point wise spectrum is not calculated) and generates resonance-corrected multigroup cross sections. Note that the NITAWL module, which uses the Nordheim Integral Method, is omitted here.

The double heterogeneity (caused by shadowing effects of the fuel particles and fuel zones of the pebbles) is treated by first calculating the point-wise flux disadvantage factors for the particle-matrix unit cell and then using these factors to create the homogenized point-wise particle/matrix mixture cross sections. The homogenized point-wise cross sections are then used in the second pass to create the final resonance-shielded multigroup cross sections that represent the fuel pebbles. Finally, deterministic calculations are performed for the given cell (TRISO or pebble) with the one-dimensional Discrete Ordinates code XSDRNPM. In this eigenvalue calculation a white boundary condition is used on the outer surface.

During a PEBBED calculation, the SCALE-6 input files are updated for local temperature and burnup. To this end 42 different material zones have been defined, 30 of which are in the pebble bed region of the reactor (the core zone is divided into 3 radial and 10 axial zones), 2 zones are used to represent the control rod, 1 is used for the void region, and the remaining 9 are used for the reflector regions. The void region on top of the pebble bed is modeled using directional diffusion coefficients. The control rod is modeled by using an equivalent boron concentration. A simplification to the model is made by modeling the side void (air gap) and reactor pressure vessel as graphite.

It was chosen to perform the PEBBED full-core calculation in a high number of energy groups (12), since intermediate calculations between the pebble level and the full core calculations are omitted. Furthermore, the depletion calculation in PEBBED uses the zone-wise energy spectrum of the full core calculation to perform the zone-wise depletion. Therefore, it is attractive to retain a relatively fine group energy structure, especially in the case of Pu fuel, which is characterized by the presence of important low-lying resonances.

2.1.3 DESCRIPTION OF THE THERMIX CODE

Thermal-hydraulic feedback is provided using THERMIX-KONVEK [8], which utilizes the power density profile calculated by PEBBED and computes the average temperature for each material zone. This temperature is then used in the cross section preparation step in SCALE-6 in which each zone is treated separately.

THERMIX is a 2-D thermal hydraulics code that consists of a heat conduction (and thermal radiation) part and a part for fluid convection. In the latter, the pressure field of the moving fluid for a 2-D cylindrical configuration is solved by linking the equations for conservation of mass and momentum. In the first part of the code the energy conservation equation is solved for steady state or time-dependent cases and applied to the solid phase material. The two parts are coupled by a source term that represents the heat transfer between the solid and the fluid.

The pebble bed is treated as a (porous) homogeneous material, having an effective conductivity based on the Zehner-Schlünder relation. In this relation not only conductivity through touching pebbles is taken into account, but also radiation between the pebbles and a convective effect caused by mixing of the helium fluid in the direction perpendicular to the flow direction.

At the boundary of the conduction model a fixed temperature (side) or an adiabatic boundary condition (top and bottom) is prescribed. For the convection model, the coolant inlet temperature and outlet pressure are used as boundary conditions.

2.2 FUEL PERFORMANCE ANALYSIS CODE: PASTA

The PASTA code [16] describes the mechanical behavior of TRISO particles during irradiation and aims at calculating the coating stresses and the corresponding failure probabilities. PASTA embodies a one-dimensional analytical and multi-layer model that takes into account the visco-elastic behavior of the

coating layers and the surrounding graphite during irradiation. The main source of stress in all layers is due to the pressure build-up from the gaseous fission products in the buffer layer resulting in a radial stress on the IPyC. Moreover, the Pyrocarbon (IPyC and OPyC) layers exhibit radiation-induced dimensional changes and creep (in the radial and tangential directions). Finally, the model allows thermal expansion of all layers. PASTA solves the general stress strain equations, which include the aforementioned effects. The internal pressure in the coated particle results from gaseous fission products (Xe and Kr) that accumulate in the kernel and diffuse to the buffer layer during irradiation. The diffusion of gaseous fission products can be calculated both analytically and numerically by solving the time-dependent fission product diffusion equation. The resulting pressure (from both fission products and CO accumulation) on the IPyC layer is calculated as a function of the kernel temperature and the buffer volume with the Redlich Kwong equation of state.

Boundary conditions for the stress analysis, such as the histories of the fuel kernel temperature, the Xe and Kr source terms, the (fast) neutron dose level and the fuel burnup are provided by the PEBBED code.

3. PERFORMANCE OF AN HTR-MODULE PEBBLE-BED REACTOR LOADED WITH DEEP-BURN FUEL

The HTR-MODULE reactor has been analyzed using the PEBBED code system. Key results of the core performance are presented in Table 4 for both the DB and the reference HTR-MODULE design. The latter uses 7 g of Uranium per pebble with an enrichment of 7.8 % in U-235.

3.1 CORE PERFORMANCE DURING NORMAL OPERATION

The power profile in the DB core is slightly more peaked towards to the top of the core (see Figure 2 and Figure 3) than the reference design, though it must be noted that the location of the peak has shifted from the core radial center in the reference core to the outer region in the DB core. In the axial direction the power peak matches the low coolant temperature in the top region of the core. The DB power profile is advantageous during normal operation of the reactor. This pattern results in a lower fuel temperature in the average pebble for the DB core as compared to the reference core. However, the peak temperature that a given pebble experiences during the irradiation in the core is higher in the DB core. This results from the different burnup characteristics of the DB fuel, in which a high burnup is achieved in the very first pebble circulation (of 15 circulations in total). Because of the high loading and discharge burnup in the DB core, the fast fluence level attained is more than twice the level of the reference case. However, the maximum fast fluence level of 8.0×10^{21} cm^{-2} is not exceeded.

Typical criteria for the fuel temperature prescribe a maximum of 1523 K during normal operation. It can be seen that the Deep-Burn core operates within this limit. Effective destruction of the initial Pu is achieved. However, the burnup level is not high enough to reduce the initial Am loading. It can be seen from Figure 4 that while the initial Am-241 is effectively reduced, the amount of Am-243 increases through the transformation of Pu-242.

Table 4. Key performance parameters of the reference and the DB HTR-MODULE core designs.

Performance parameter	Deep-Burn fuel	Reference fuel UO_2
Maximum fuel temperature	1078 K	1134 K
Pebble peak temperature	1422 K	1133 K
Maximum power density	7.3 MW/m^3	5.6 MW/m^3
Fuel burnup at discharge	666 MWd/kg IHM	89 MWd/kg
Pu discharge concentration (relative to initial)	18.5 %	-
Am discharge concentration (relative to initial)	108.5 %	-
Pebble Fast (E > 0.1 MeV) fluence level at discharge	5.7×10^{21} cm^{-2}	2.1×10^{21} cm^{-2}

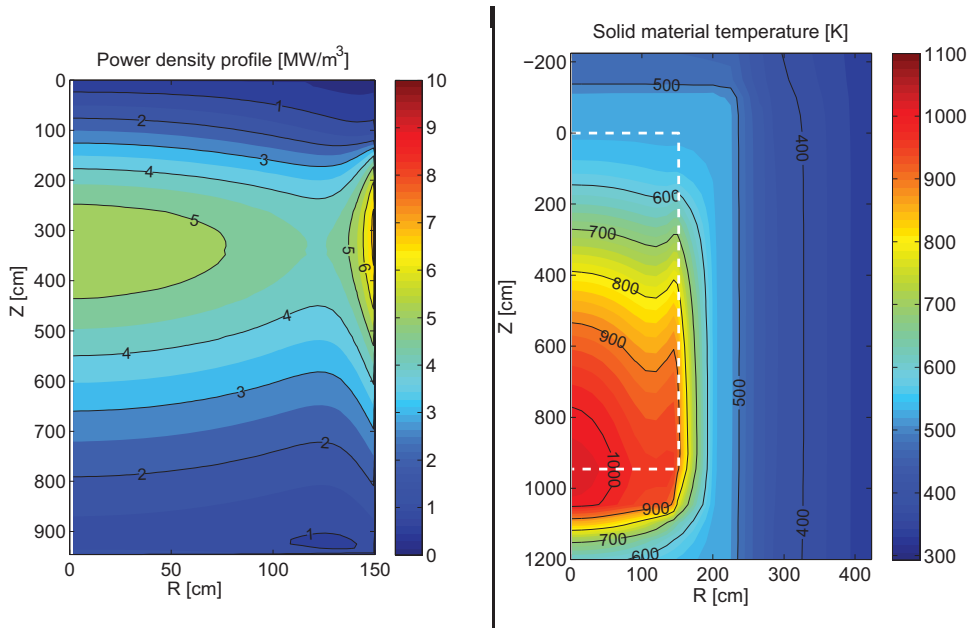

(a) (b)

Figure 2. (a) Power density profile in the *core* of the DB pebble-bed HTR-MODULE (15 pebble circulations); and (b) the temperature profile for the *entire reactor* DB HTR-MODULE (dotted line shows the boundary of the pebble-bed core).

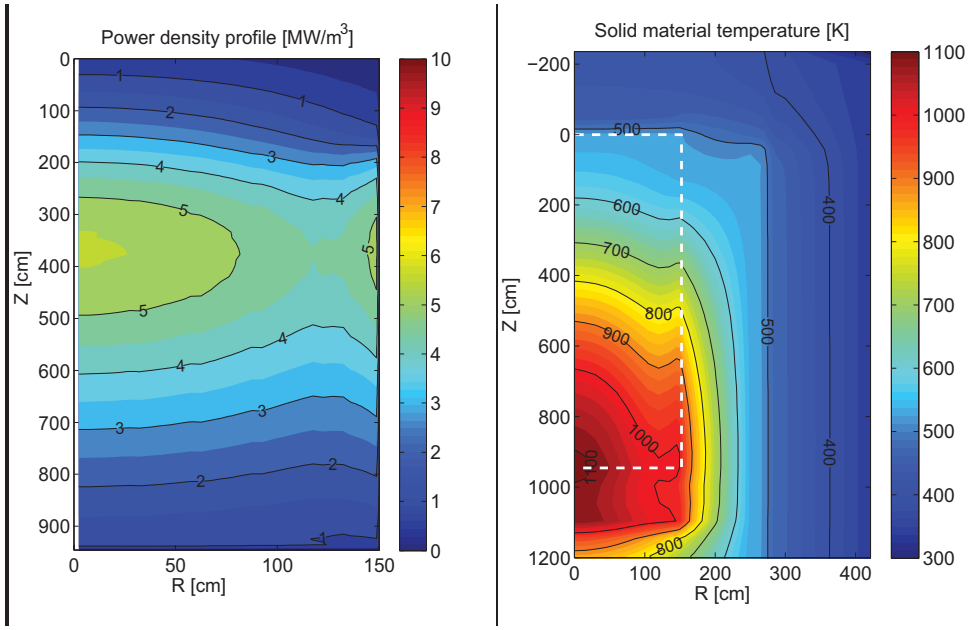

(a) (b)

Figure 3. (a) Power density profile in the pebble-bed *core* of the reference HTR-MODULE (15 pebble circulations); and (b) the temperature profile for the *entire* reference HTR-MODULE *reactor* (dotted line shows the boundary of the pebble-bed core).

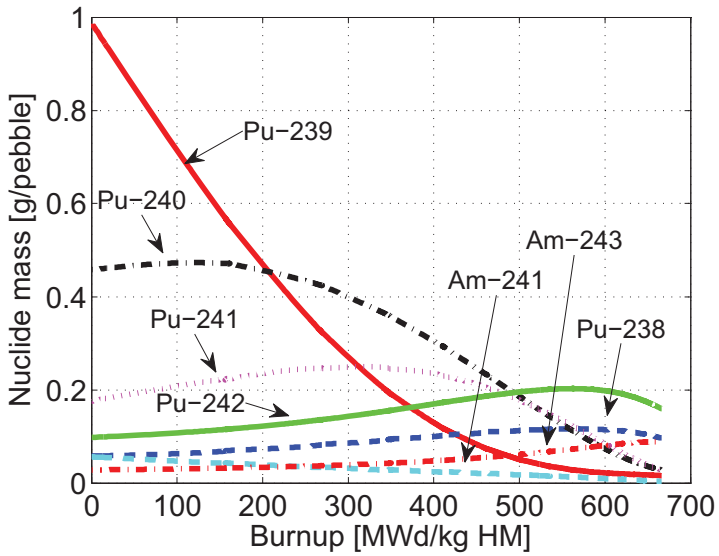

Figure 4. Histories of the mass of relevant Pu and Am nuclides during irradiation in the DB HTR-MODULE 200 MW_{th} design.

3.2 CORE PERFORMANCE FOR A LOSS OF FORCED COOLING INCIDENT

The performance of the HTR-MODULE during a Loss Of Forced Cooling incident has been investigated for both UO_2 and DB fuel types. For this transient case it is assumed that the coolant mass flow is reduced instantaneously to zero and that the system pressure is reduced from 6 MPa to atmospheric pressure.

Assuming a reactor SCRAM the power is determined by the decay heat only. The 'standard' decay heat curve that is supplied by THERMIX (Figure 5) is assumed for the UO_2 loaded core, while a typical DB decay heat curve was also implemented in the code for the analysis of the DB fueled core.

After the initiation of the transient, the core starts to heat up by deposition of the decay heat in the absence of forced cooling. The fuel (maximum and core-average) temperature response for this transient is presented in Figure 6 (a). Heat from the core is transferred to the Reactor Heat Removal System (RHRS) that surrounds the RPV from a distance of 1 m. These water panels are assumed to be at a constant temperature of 70 ºC. Heat from the pebble bed core is transferred by conduction and thermal radiation to the side reflector. Heat is conducted through the reflector and the RPV, where thermal radiation effectively transfers the heat to the RHRS.

After the initial temperature rise, the core starts to cool down at the point when the decay heat equals the amount of heat transferred to the RHRS. The UO_2-fueled MODULE reaches a maximum fuel temperature of 1499 ºC after 27.5 h, while the DB-fueled core reaches its maximum of 1421 ºC only after 68.5 h. Figure 7 shows the core temperature profiles for both fuel types at the time the maximum fuel temperature is attained. The figure shows that only a small part of the core is at this high temperature. This is also reflected in the volume weighted average core temperature, which reaches maximum values of only 837 ºC and 821 ºC, for the UO_2 and DB fuel types, respectively.

Although the temperature trends and profiles are similar, some differences can be identified between the two fuel types (Figure 6 and Figure 7). The shape of the DB power profile, with a peak at the radial outer

surface instead of at the center, is advantageous during the LOFC transient. Furthermore, temperature-dependent conductivities for graphite were used in the DB core analysis, which are higher than the conservative fixed value of 26 W/m/K that was used for the UO_2 fueled case. Consequently, the maximum temperatures reached in the DB case are lower and the radial temperature profile in the side reflector is different. Applying the more conservative conductivity value to the DB, would result in an increase of the maximum fuel temperature by 59 ºC to 1480 ºC. Even for this more conservative case the maximum fuel temperature stays well within the generally accepted limit of 1600 ºC.

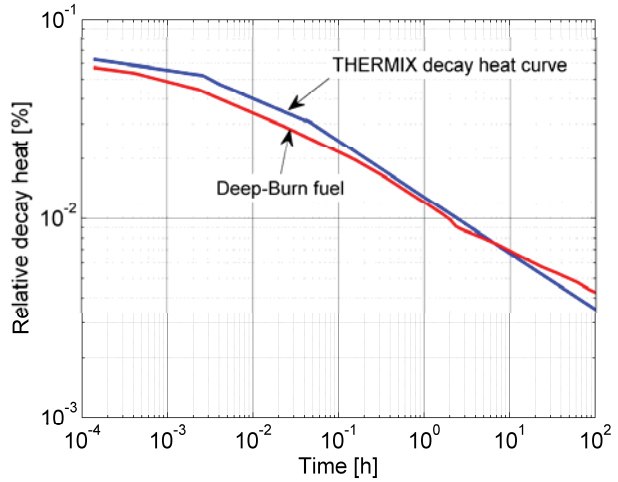

Figure 5. Decay heat curve in THERMIX and a decay heat curve calculated using ORIGEN-S for typical Deep-Burn fuel.

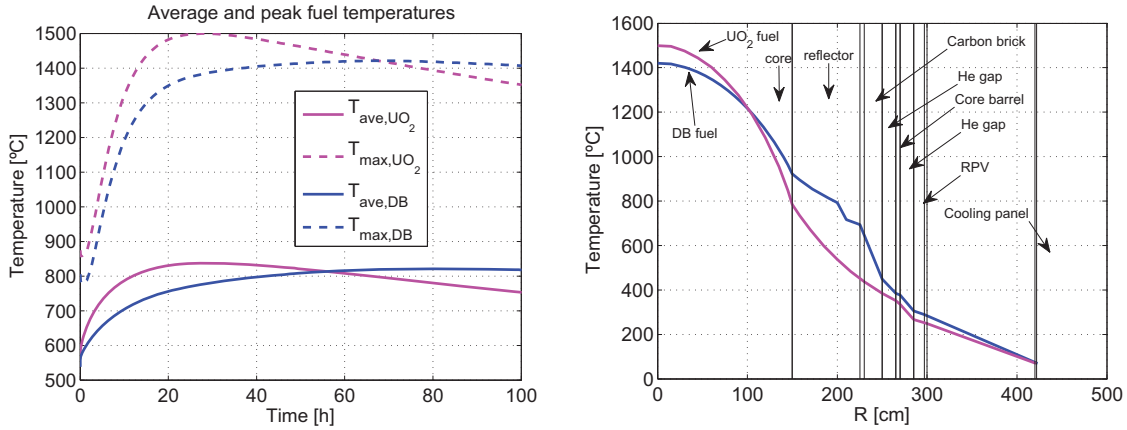

(a) (b)

Figure 6. Maximum and core-average fuel temperature histories for the reference UO_2-fueled HTR-MODULE and the DB fuel design (a). Radial temperature profile at *the axial position* and at *the time* of the maximum core temperature for both core designs (b).

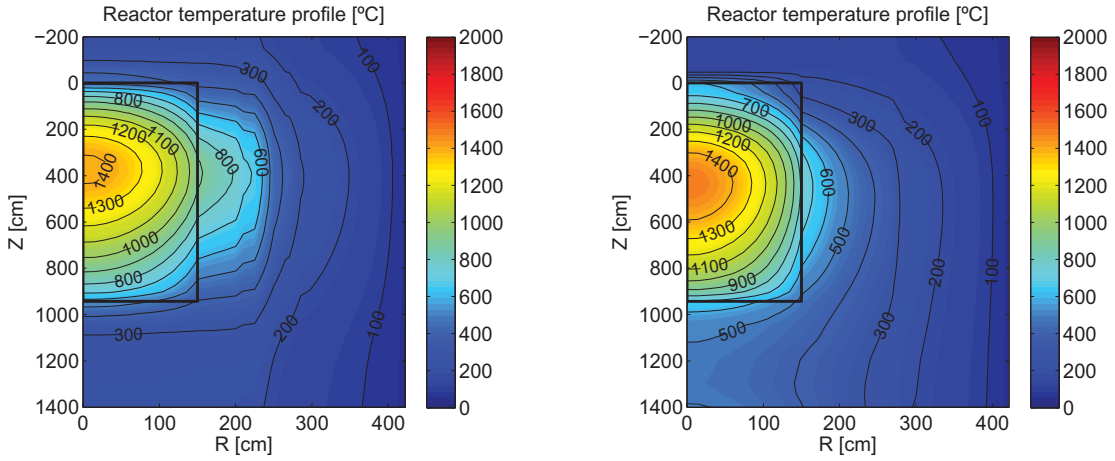

(a) (b)

Figure 7. Temperature profile in the HTR-MODULE at the time of the peak temperature during a DLOFC transient, for a DB design (a) and for the reference UO_2 design.

4. INCORPORATION OF A MODIFIED OPEN FUEL CYCLE COMPONENT IN THE DEEP-BURN PEBBLE-BED REACTOR FUEL

4.1 SELECTION OF NUCLIDES FOR INCORPORATION IN DEEP-BURN FUEL

Besides the use of Pu and Minor Actinides (MA) from used Light Water Reactor (LWR) fuel in the Deep-Burn (DB) concept, additional nuclides from the nuclear waste stream could be incorporated in the DB fuel to improve the fuel cycle. The incorporation of Long Lived Fission Products (LLFP) in the fuel, and their destruction by irradiation in the DB core, would reduce the radiotoxicity of the final nuclear waste product at long storage times ($t > 10^5$ years) [10]. Furthermore, short lived fission products (gamma emitters) could be incorporated in the fuel to make it more proliferation resistant.

Table 5 presents important characteristics of the LLFP and Cs-137 that can be found in LWR used fuel. The latter could be included in the DB fuel as a proliferation resistant measure, since its decay results in a strong gamma emitter (Ba-137m). Figure 8 shows the impact of the LLFP on the radiotoxic inventory of typical used LWR fuel. It is noted that the Pu and MA, which are not shown in Figure 8 dominate the radiotoxic inventory up to several million years. Regarding the radiotoxic inventory of the fission products, the first 10^3 years are dominated by Sr-90 and Cs-137, while Tc-99 contributes the most to the radiotoxic (fission product) inventory beyond this time point until roughly 3×10^5 years. From that time onward the I-129 contribution dominates radiotoxicity.

For completeness the production of LLFP and Cs-137 from an HTR is also given in Table 5. Note that the amount of LLFP in used fuel is approximately linearly dependent of the burnup level. Therefore the amount of LLFP in HTR used fuel (95 MWd/kg initial Heavy Metal [HM]) is higher than in PWR used fuel (41.2 MWd/kg HM). The spectral differences between an HTR and a PWR result in small differences in the yields of the LLFP.

Table 5. Half-lives (ENDF/B-VII.0), abundance in UO_2 used fuel and dose-coefficients of selected fission products.

Nuclide	Half-life [a]	Weight fraction in used PWR fuel [2]	Weight fraction in used HTR fuel [1]	Effective dose coefficients e_{50} (ingestion) for adults [Sv/Bq] [3]	σ_t [b] (0.0253 eV, 300 K)
Se-79	3.0×10^{5}	6.0×10^{-6}	1.4×10^{-5}	2.9×10^{-9}	5.6×10^{1}
Zr-93	1.5×10^{6}	8.8×10^{-4}	2.1×10^{-3}	1.1×10^{-9}	6.5×10^{0}
Tc-99	2.1×10^{5}	1.0×10^{-3}	2.4×10^{-3}	6.4×10^{-10}	2.9×10^{0}
Pd-107	6.5×10^{6}	2.7×10^{-4}	6.4×10^{-4}	3.7×10^{-11}	5.3×10^{0}
Sn-126	2.3×10^{5}	3.0×10^{-5}	5.4×10^{-5}	4.7×10^{-9}	4.1×10^{0}
I-129	1.6×10^{7}	2.1×10^{-5}	4.2×10^{-4}	1.1×10^{-7}	4.1×10^{1}
Cs-135	2.3×10^{6}	4.7×10^{-4}	8.6×10^{-4}	2.0×10^{-9}	1.5×10^{1}
Cs-137	3.0×10^{1}	1.3×10^{-3}	3.6×10^{-3}	1.3×10^{-8}	3.8×10^{0}

[1] UO_2 fuel at 95 MWd/kg HM burnup from a High Temperature Reactor calculated with SCALE-6.
[2] UO_2 fuel at 41.2 MWd/kg HM, initial fuel 3.7 % enriched in U-235, 4 years cooling time [10].
[3] Data taken from ICRP 72 [11].

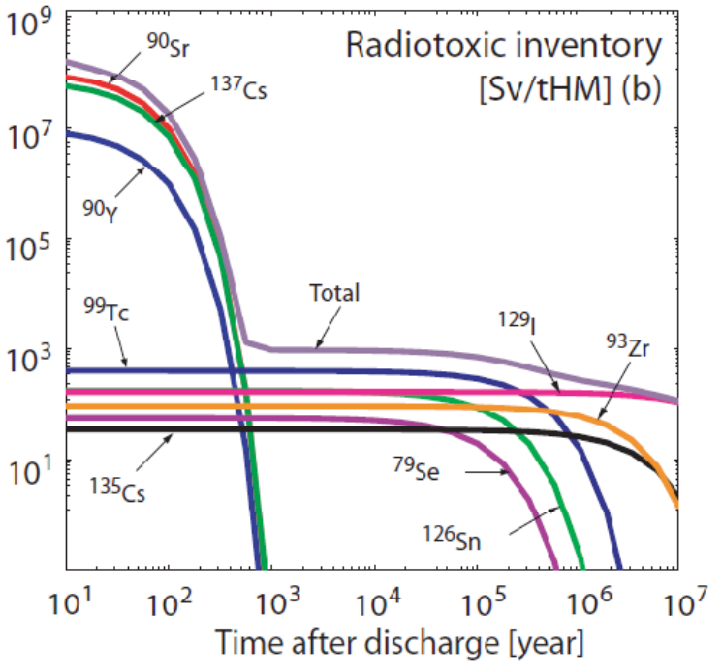

Figure 8. Radiotoxic inventory of fission products in used (41.2 MWd/kg HM) LWR fuel [10]. Taken from Tucek [12].

The total neutron cross section at a thermal energy of 0.0253 eV is listed for the considered nuclides in the last column of Table 5 and the cross sections as a function of neutron energy are given in Figure 9. On the one hand a large cross section is advantageous, since it would allow for effective destruction of the

LLFP. The downside of this is of course the increased 'parasitic' absorption, which will result in a reduction of the achievable discharge burnup of the fuel. In particular, it can be seen that Se-79, I-129, Tc-99 and Cs-135 possess a relatively large cross section.

The presence of resonances is advantageous with respect to the temperature reactivity coefficient (Doppler Effect). In general the lowest-lying resonance characterizes the temperature coefficient from the Doppler broadening perspective. It can be seen that Tc-99 has a large resonance at a relatively low energy (5.6 eV). Besides the Doppler Effect, an increase of the moderator material temperature would result in a shift of the peak of the thermal spectrum to higher energies with consequent increased absorption in the lower end of the resonance. This leads to an improvement of the moderator temperature coefficient.

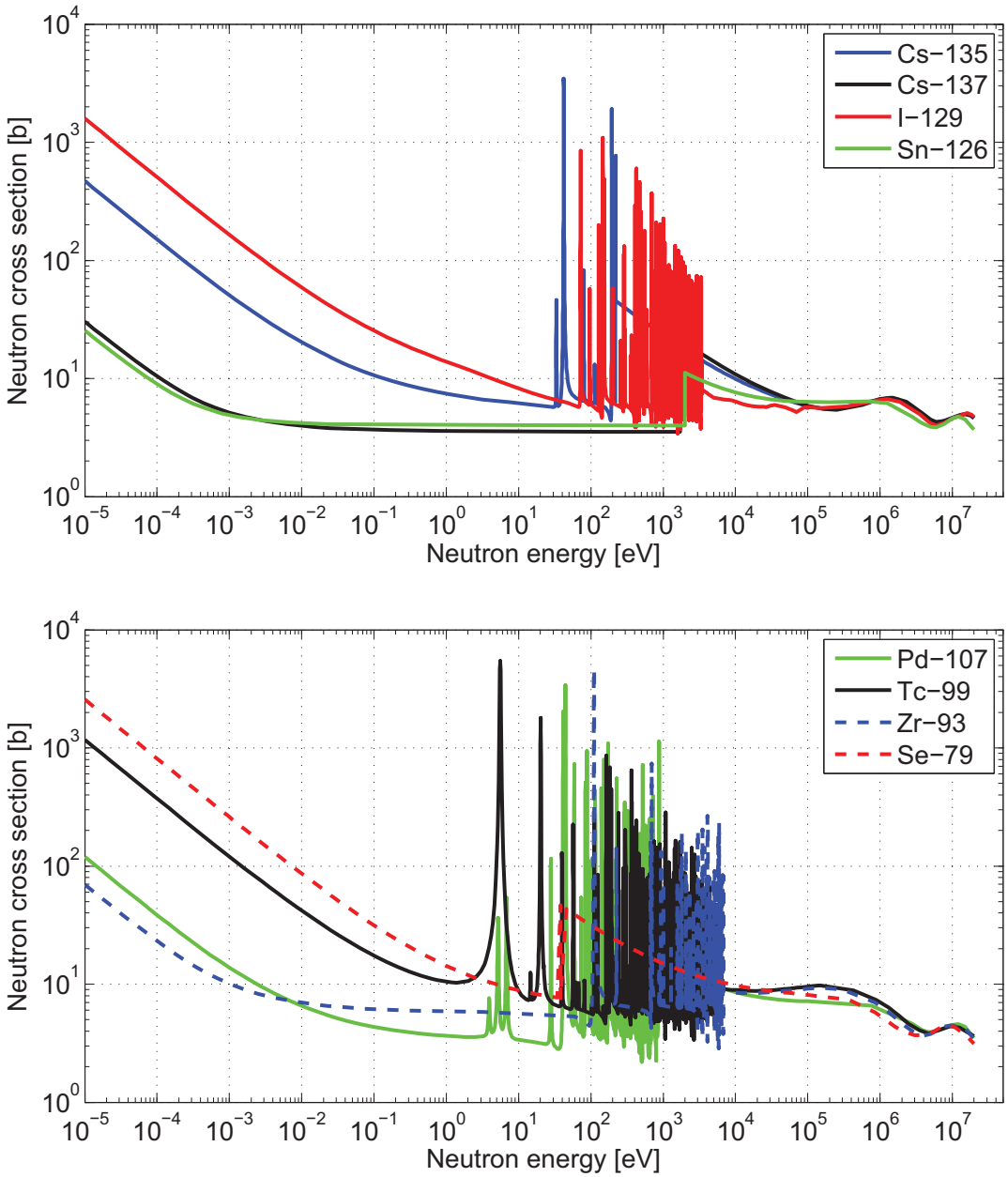

Figure 9. Neutron cross sections (total) of LLFP and Cs-137 taken from ENDF/B-VII.0 nuclear data.

4.2 ANALYSIS RESULTS FOR A HTR-MODULE LOADED WITH DB FUEL AND LLFP

In this section it will be shown by how much the initial LLFP content can be reduced. The section also discusses the effects on the achievable discharge burnup and on the temperature coefficient of the incorporation of LLFP nuclides into the DB fuel..

Three cases have been analyzed with a loading of 0.1 g, 0.5 g and 0.7 g of LLFP per pebble, respectively, in dedicated TRISO particles. These LLFP-TRISO particles are embedded within the same pebble as the DB fuel TRISO particles that constitute the 2g per pebble of HM.

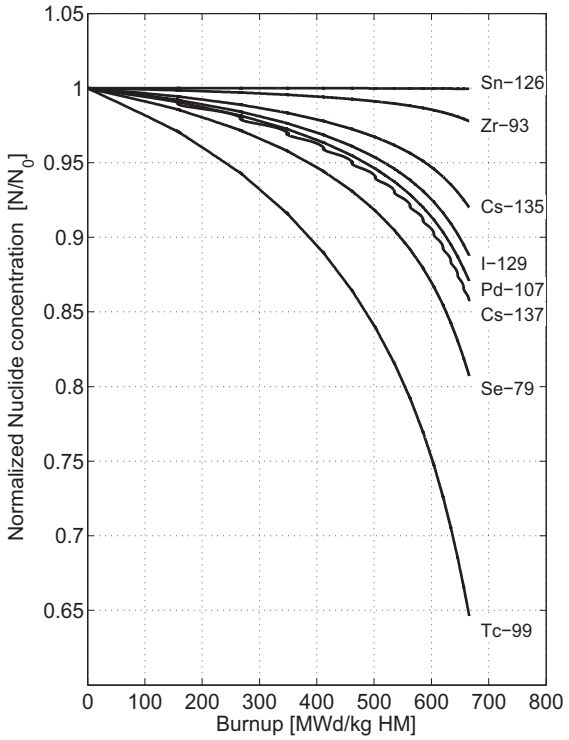

Figure 10. Histories of the nuclide concentrations of the LLFP normalized to their initial concentrations as function of the HM burnup. The loading of LLFP is 0.1 g per pebble.

Figure 10 shows the histories of the concentrations of the LLFP as a function of the fuel burnup for a loading of 0.1g LLFP per pebble. As could be expected from the neutron cross sections of Figure 9 the concentrations of Tc-99 and Se-79 are reduced especially more significantly than the other LLFPs. The absorption cross section of Cs-137 is relatively small, but its concentration is reduced by radioactive decay. The reduction of I-129 shown in Figure 10 is not as large as one would expect intuitively from looking at Figure 9. However, the capture cross section of I-129 shows a drop-off between 1 eV and 100 eV, where Pd-107 and Tc-99 have significant capture resonances. These latter nuclides appear to contribute significantly to the effective capture cross section in the neutron energy spectrum of the HTR-DB core. Other mechanisms, yet to be studied, such as competing mechanisms, may be contributors to the low destruction level for I-129.

Although a high burnup level can still be reached at this low LLFP loading, the destruction of LLFP is disappointing. The only nuclide that is reduced significantly (more than 35 % reduction) is Tc-99. Table 6 shows the initial and discharge mass of the relevant Pu & MA and LLFP. The total amount of LLFP is reduced from 0.1 g per pebble to 0.0834, which is mainly due to the reduction in Tc-99. The influence of the LLFP on the achievable discharge burnup of the Pu & MA is negligible at this low loading of LLFP.

Table 6. Initial and discharge masses of selected nuclides.

Isotope	Initial loading (g/pebble)	Discharge (g/pebble)
^{237}Np	0.136	0.0313
^{238}Pu	0.0580	0.0965
^{239}Pu	0.987	0.0157
^{240}Pu	0.458	0.0285
^{241}Pu	0.176	0.0285
^{242}Pu	0.0980	0.160
Pu total	1.78	0.329
^{241}Am	0.0560	0.00359
^{242m}Am	0.00040	0.0000852
^{243}Am	0.0280	0.0882
Pu+MA total	2.00	0.452
^{79}Se	0.000151	0.000121
^{93}Zr	0.0222	0.0217
^{99}Tc	0.0251	0.0162
^{107}Pd	0.00680	0.00592
^{126}Sn	0.000755	0.000754
^{129}I	0.000528	0.000469
^{135}Cs	0.0120	0.0103
^{137}Cs	0.0327	0.0280
LLFP total	0.100	0.0834
^{167}Er	0.0257	0.000002

Key core performance parameters are compared for the three different amounts of LLFP loadings per pebble in Table 7. With increasing LLFP loading the power peak at the radial outer surface of the pebble bed becomes more dominant. This change in shape of the power profile is advantageous when the loading is increased from 0.1 g to 0.5 g, resulting in a lower maximum fuel temperature. If the loading is increased further to 0.7 g, a high temperature at the core outer surface is experienced, which is higher than the maximum value that was previously located at the radial center of the core.

The parasitic neutron absorption increases with the LLFP loading per pebble. As a result the achievable discharge burnup decreases. Since the discharge burnup is a function of the pebble residence time in the core, the fast fluence level attained is the lowest for the highest LLFP loading.

The maximum fuel temperature experienced during the LOFC transient is the lowest for the case with the highest LLFP loading. This case has also the highest discharge burnup and as a result the highest power peak at the core outer surface. The latter is advantageous during the LOFC transient with regard to the maximum fuel temperature.

The temperature coefficient of reactivity has been calculated with the SCALE-6 code system. The average nuclide concentrations have been taken from the PEBBED analysis for the equilibrium core composition and are used in a lattice cell calculation for the pebble bed at several temperatures. In general, the following three temperature coefficients are considered in pebble-type fuel:

- the Fuel Temperature Coefficient (FTC), which is concerned with reactivity effects resulting from a temperature change of the fuel kernels;
- the Moderator Temperature Coefficient (MTC), which is related to temperature changes of the graphite matrix in which the coated particles are embedded and the graphite outer shell of the pebble;
- and the Uniform Temperature Coefficient (UTC), which is related to temperature changes of the pebble as a whole.

Previous studies showed that for DB fuel, the MTC is much larger than the FTC and is close to the UTC. It becomes less negative (and even positive for some conditions) with increased burnup. This is the result of the differences in interplay between the shift in the neutron energy spectrum and the low-lying resonances of Pu-239 and Pu-241. Furthermore, the concentration of Er-167, which is added to the fuel kernel to improve the MTC, reduces with increasing burnup. Therefore, the cases with the higher LLFP loadings (lower burnup) have a Uniform Temperature Coefficient (UTC) that is more negative.

The presence of the LLFP in the pebble slightly improves the UTC. For the case with 0.7 g LLFP per pebble the UTC at the pebble-cell level would increase from -5.9 to -5.4 pcm/K (at 500 K) if the LLFP are not taken into account. The improvement in the UTC by the addition of LLFP is mainly attributable to Tc-99. This nuclide has an important low-lying resonance near the thermal energy range, which gives a negative contribution to the MTC.

Table 7. Key core performance parameters for LLFP loadings per pebble of 0.1 g, 0.5 g and 0.7 g.

Parameters	0.1 g LFFP/peb.	0.5 g LLFP/peb.	0.7 g LLFP/peb.
Maximum fuel temperature	1077 K	1065 K	1090 K
Maximum power density	7.3 MW/m^3	7.9 MW/m^3	9.4 MW/m^3
Fuel burnup at discharge	665 MWd/kg	630 MWd/kg	534 MWd/kg
Pu discharge concentration (relative to initial)	18.5 %	22.9 %	34.9 %
Am discharge concentration (relative to initial)	109 %	112 %	115 %
LLFP discharge concentration (relative to initial)	83.9 %	86.7 %	88.7 %
Pebble Fast (E > 0.1 MeV) fluence level at discharge	5.77 x $10^{21}cm^{-2}$	5.64 x $10^{21}cm^{-2}$	4.48 x $10^{21}cm^{-2}$
Uniform Temperature coefficient at 875 K	-11.6 pcm/K	-11.9 pcm/K	-12.0 pcm/K
Uniform Temperature coefficient at 500 K	-4.0 pcm/K	-5.9 pcm/K	-5.9 pcm/K
DLOFC Maximum fuel temperature	1693 K	1655 K	1630 K

4.3 CONCLUSION ON THE USE OF LLFP IN COMBINATION WITH DB FUEL

The results of the analysis show that LLFP can be incorporated in the pebbles of a DB–loaded HTR-MODULE reactor without compromising the safety parameters of the reactor. The fuel temperature and power peaking are comparable to the reference DB MODULE core, for which the pebble peak temperature does not exceed the limit of 1523 K for normal operation. The maximum temperature during a LOFC remains well below the generally accepted limit of 1873 K and the maximum fluence levels stay below the limit of 8.0 x 10^{21} cm^{-2}.

The destruction capability for the LLFP in the DB-MODULE reactor is however limited. Only Tc-99 seems to be effectively reduced. To achieve significant reduction of the LLFP or just compensation for their formation within the fuel particles, which amounts to about 0.18 g, a higher loading would be required. This would in turn reduce the achievable discharge burnup. This finding implies that the use of LLFP in the pebbles of an HTR-MODULE reactor is not justified, especially if one takes into account the increase in expense associated with a more complex fuel fabrication process, which is most likely to occur. Only the addition of Tc-99, which can be effectively reduced and also provides an improvement of the temperature coefficient, should be investigated further.

5. INCORPORATION OF AMERICIUM TARGETS IN THE DEEP-BURN PEBBLE-BED REACTOR

Americium causes the second highest contribution to the radiotoxic inventory of LWR fuel next to that of Plutonium (Figure 11). It can be seen from Figure 11 that the Am radiotoxicity results mainly from the Am-241 isotope and lasts until 4 x 10^3 years after discharge. This is the result in large part of the β^- decay of Pu-241 (half-life of 14.35 years) to Am-241. Am-243 determines the radiotoxicity of Am for times beyond 4 x 10^3 years.

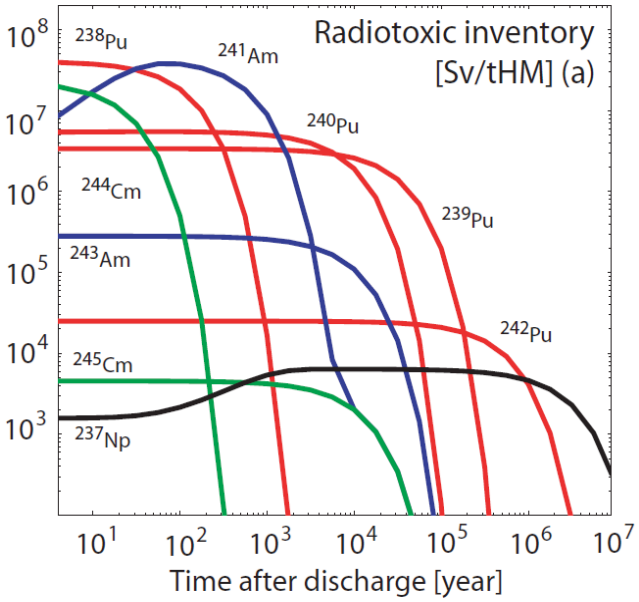

Figure 11. The radiotoxic inventory of transuranics in LWR (41.2 MWd/kg HM) LWR fuel [10]. Taken from Tucek [12].

The alpha-decay of Am-241 gives, besides a high contribution to the radiotoxicity, a high decay heat load and significant He production. The latter is mainly due through indirect α-decay through Cm-242. If recycled, this isotope can lead to challenges to reactor and fuel performance, while the heat load would have consequences for the waste repository requirements in the case of direct disposal. Studies regarding LWRs show that recycling of Am can lead to a reduction of the achievable discharge burnup and a less negative moderator temperature coefficient [10]. This is the result of the large neutron cross sections of the Am isotopes, including significant resonances in the thermal energy range (Figure 12).

5.1 ANALYSIS RESULTS OF A HTR-MODULE LOADED WITH DB FUEL AND AM-TARGETS

Using the PEBBED code system, an investigation has been carried out of several important core parameters. In this study the amount of Am in dedicated coated particles was varied between 0.1 and 0.3 g per pebble.

The key results of the analysis are given in Table 8. For the isotopic composition of the Am particles the weight fractions of Table 3 are used. Similarly to what was observed with the addition of LLFP, the discharge burnup of the fuel decreases as the loading of Am-containing particles is increased.

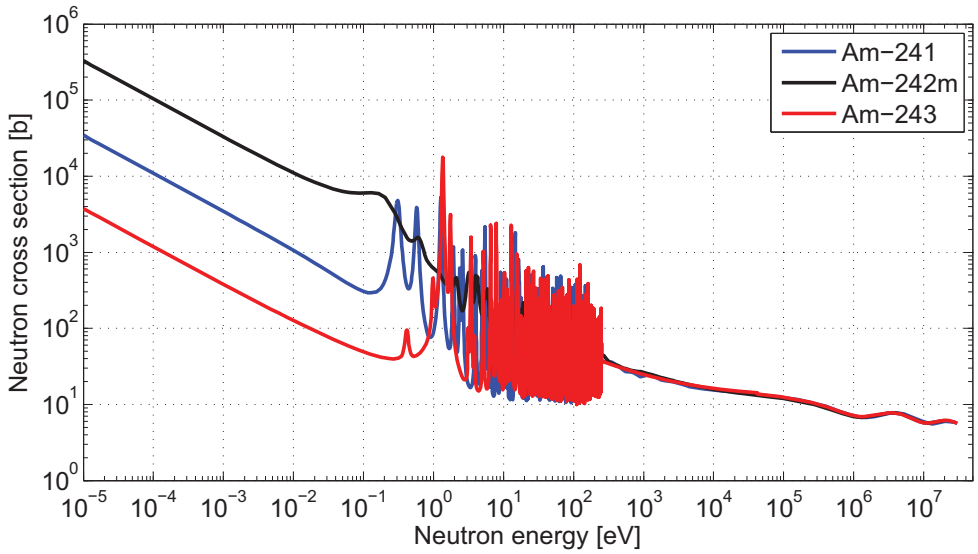

Figure 12. Neutron cross sections (total) of Am-241, Am-242m and Am-243 taken from ENDF/B-VII.0 nuclear data.

The highest Am loading results in a significantly higher fuel temperature during normal operation. However, the temperature does remain within acceptable limits. This can be attributed to the larger power peaking at the core outer surface, which in turn results in a lower maximum fuel temperature during the DLOFC transient.

Note that the same (DB) decay heat curve was used as in the previous analysis for the DLOFC transient calculations. The addition of extra Am is expected to increase the decay heat leading to higher fuel temperatures than reported in Table 8.

Table 8. Key core performance parameters for Am loadings per pebble of 0.1 g, 0.2 g and 0.3 g.

Parameters	0.1 g Am/peb.	0.2 g Am/peb.	0.3 g Am/peb.
Maximum fuel temperature	1079 K	1072 K	1111 K
Maximum power density	7.3 MW/m^3	7.7 MW/m^3	10.1 MW/m^3
Fuel burnup at discharge	682 MWd/kg	662 MWd/kg	508 MWd/kg
Pu discharge concentration (relative to initial)	16.4 %	18.7 %	37.6 %
Am discharge concentration (relative to initial)	120 %	60.4 %	51.0 %
Pebble Fast (E > 0.1 MeV) fluence level at discharge	5.72 x $10^{21}cm^{-2}$	5.76 x $10^{21}cm^{-2}$	4.25 x $10^{21}cm^{-2}$
Uniform Temperature coefficient at 875 K	-11.0 pcm/K	-11.9 pcm/K	-10.2 pcm/K
Uniform Temperature coefficient at 500 K	-3.5 pcm/K	-5.25 pcm/K	-7.0 pcm/K
DLOFC Maximum fuel temperature	1715 K	1682 K	1631 K

6. CORE PERFORMANCE OF A PEBBLE-BED REACTOR FUELED WITH URANIUM AND DEEP-BURN FUEL

The addition of Uranium to DB fuel can possibly lead to an improvement of the temperature coefficient. This claim is the result of intuitive considerations on the increased in resonance absorption that results from the presence of the U-238 isotope, which is known to result in increased neutron absorption at increased temperatures. However, the absorption in U-238 also leads to the production of Pu-239, which in turn partly offsets the destruction of Pu-239 in the DB fuel. In the following section, the results of a PEBBED analysis are given that quantify the consequences of Uranium addition to DB fuel.

6.1 ANALYSIS RESULTS OF A HTR-MODUL LOADED WITH DB FUEL AND URANIUM

Table 9. Key core performance parameters for U loadings per pebble of 0.5 g, 1.0 g, 1.5 g and 2.0 g.

Parameters	0.5 g	1.0 g	1.5 g	2.0 g
Maximum fuel temperature	1069 K	1053 K	1102 K	1172 K
Maximum power density	7.7 MW/m^3	8.4 MW/m^3	10.0 MW/m^3	11.5 MW/m^3
Fuel burnup at discharge	652 MWd/kg	616 MWd/kg	521 MWd/kg	399 MWd/kg
Pu discharge concentration (relative to initial)	21.5%	27.2%	40.7%	56.6%
Am discharge concentration (relative to initial)	110.0%	114.2%	118.6%	117.9%
Pebble Fast (E > 0.1 MeV) fluence level at discharge	5.8 x $10^{21}cm^{-2}$	5.7 x $10^{21}cm^{-2}$	4.6 x $10^{21}cm^{-2}$	3.5 x $10^{21}cm^{-2}$
Uniform Temp. coefficient at 875 K	-12.4 pcm/K	-12.8 pcm/K	-11.9 pcm/K	-10.9 pcm/K
Uniform Temperature coefficient at 500 K	-5.8 pcm/K	-7.8 pcm/K	-8.3 pcm/K	-8.5 pcm/K
DLOFC Maximum fuel temperature	1678 K	1651 K	1619 K	1610 K

From Table 9 it can be seen that by adding Uranium to the pebble the temperature coefficient becomes more negative, as expected. However, the achievable discharge burnup decreases with increasing U loading. Furthermore, the effectiveness of the Pu and MA destruction is reduced since some new Pu and MA build up in the Uranium bearing particles (Figure 13).

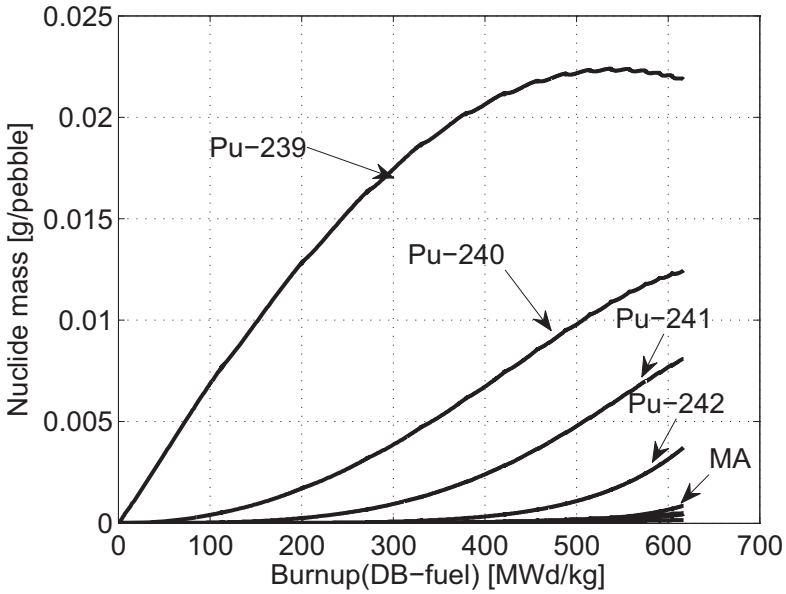

Figure 13. Formation of Pu and MA in the U-fuel particles of pebble loaded with 2g DB-fuel and 1g Uranium.

7. CONCLUSIONS

This conclusion presents the main findings of the Deep Burn Pebble Bed concept investigation. The most recent studies (carried out since September 2010) were presented above. A number of additional studies (carried out previously and either not documented or only partly documented) as well as details of the studies presented above and supporting models and method descriptions are given as Appendices following this conclusion. When a conclusion is presented in this section but related information does not appear above in the body of this report, then the supporting information is given in one of the Appendices that follow.

The findings presented in this section are organized into two categories (and corresponding subsections): conclusions regarding the analysis and design of the Deep Burn PBR core and conclusions regarding the analysis and design of the DB coated particle fuel.

7.1 CONCLUSIONS REGARDING THE ANALYSIS AND DESIGN OF THE DEEP-BURN PEBBLE-BED CORE

- *Use of Erbium and increased fuel loading for improvement of the temperature reactivity coefficient*

The problem of poor temperature reactivity coefficients is identified in Appendix A-1 and the approach to remedy the situation and the related detailed analyses are shown in Appendix A-2. To improve the moderator temperature coefficient both the addition of Er-167 to the pebble or fuel kernel as well as an increase in the fuel loading per pebble have been considered. It was found that the Uniform Temperature coefficient can be rendered negative for the entire core and for the entire temperature domain by the addition of Er-167 to the fuel kernel. The resulting penalty on the achievable discharge burnup is ~100 MWd/kg. This would result in an achievable discharge burnup of 600 MWd/kg from the Pu-only fuel performance.

Analyses in which the location of the Erbium within the pebble was varied, showed that the Erbium could be effectively (self-) shielded in the beginning of the irradiation. As a consequence more Erbium would be available later in the irradiation, i.e., at high burnup levels, where it would be most effective in improving the temperature coefficient.

Alternatively to Erbium addition, the analysis shows that increasing the HM load from 2 to 3 g per pebble without burnable poison addition is the most attractive option with regard to the discharge burnup. It would keep the discharge burnup above 690 MWd/kg, while keeping the maximum UTC below -1 pcm/K.

- *Low density inner reflector or no inner reflector reduces power and temperature peaking in the core*

To mitigate power peaking in the core, both an annular core with a neutronically transparent inner reflector and a cylindrical core were examined and found to yield an improvement. However, the first alternative demands a low effective graphite density ($\rho < 0.2\rho_0$), which might be difficult to achieve in practice. The latter demands a reduction in the total reactor power, since cylindrical cores are less effective at heat removal during a Depressurized Loss Of Forced Cooling (LOFC) event. The details of the corresponding study are shown in Appendix A-3.

In Section 1 and in AppendixA-5, it is found that an alternative Deep-Burn design based on the cylindrical HTR-PM (250 MWth) can achieve a higher discharge burnup of 560 MWd/kg (using a Pu and

MA initial fuel loading). This design also exhibits lower temperature peaking (1190 K) during the first pebble pass. The maximum fuel temperature during a LOFC transient has a best estimate value of 1734 K, which is within generally accepted safety limits. It is noted that these temperature reductions are achieved at the expense of a lower helium outlet temperature (750°C), a lower reactor power (250 MW) and an increase in the number of pebble (re)circulation passes from 6 to 20.

- *Analysis of the decay heat from Deep-Burn fuel*

Decay curves for UO_2 fuel and for Pu as well as Pu+MA fuels are compared in Appendix A-4. The curves presented in that appendix go from immediately after shutdown (~10^{-4} hour) to about 100 hours. The curves are given for intermediate burnup levels and for high (discharge-like) respective burnup level for each fuel. Some observations are presented in turn, next.

Early on following shutdown, all the curves are bunched together, exhibiting similar initial decay heat behavior for the first 10^{th} of an hour. However, as time passes the curves diverge strongly, ending with differences of up to ½ to nearly one full order of magnitude after 100 hours.

Qualitatively, the decay heat curve of Deep-Burn fuel is similar to that of 'standard' UO_2 fuel at low burnup levels.

At high burnup levels (B > 600 MWd/kg) the decay heat curve is significantly influenced by the contribution of the unstable minor actinides. These nuclides give a relatively large contribution for these burnup levels, especially after several hours of decay (t > 2 hours). The decay heat curves of the two Deep-Burn fuels considered (Pu only and Pu+MA) are very similar but also diverge at high decay times (about 4.8% for Pu+MA and about 6.8% for Pu only at 100 hours). Because the Pu only fuel is able to attain a higher discharge burnup level the decay heat is also higher for this fuel type. From the transient analysis of a DB HTR-PM design, it was found that adopting a typical DB decay heat curve instead of the standard curve for UO_2 fuel would increase the maximum fuel temperature by ~100 K. It is noted here that a fixed power profile was assumed for the decay heat during the transient. This is expected to be a conservative assumption, because the decay heat core power profile will be more flattened with increased cooling time.

- *Sensitivity of the fuel temperature on the fast neutron dose*

In Appendix A-5 (Section A-5.4), the impact of the fluence level on the fuel temperature during normal and Loss Of Forced Cooling conditions has been determined. The maximum temperatures during a DLOFC are sensitive to the neutron dose levels received by the pebbles and by the side reflector. For a best estimate value of the maximum reflector dose levels that are reached in the lifetime of the reactor, the maximum core peak temperature increases by an additional 200°C to 1877°C. It is noted here that a similar increase is also to be expected for the 'standard' HTR-PM with UO_2 fuel.

- *Core analysis of a HTR-MODULE design loaded with Deep-Burn fuel*.

The cylindrical core design of the HTR-MODULE, which has a slightly lower power density than the HTR-PM design, performs well with regard to the peak temperature and the achievable discharge burnup. The achievable discharge burnup for the reference DB-fuel is 666 MWd/kg and the peak temperature during a DLOFC transients remains within the generally accepted limit of 1600°C. (See Section 3.1.)

- *Core analysis of a HTR-MODULE design loaded with Deep-Burn fuel and Uranium.*

By adding Uranium to the DB-fuel pebbles in dedicated particles the temperature coefficient of reactivity of the DB pebble-bed reactor can be improved. A reduction in the achievable discharge burnup and the amount of Pu that is reduced in the DB-fuel was found with increased U loading per pebble. (See Section 6.)

- *Core analysis of a HTR-MODULE design loaded with Deep-Burn fuel and Modified Open Cycle Components.*

The results of the analysis (see Section 4) show that LLFP can be incorporated in the pebbles of a DB – loaded HTR-MODULE reactor without compromising the safety parameters of the reactor. The fuel temperature and power peaking are comparable to the reference DB MODULE core, for which the pebble peak temperature does not exceed the limit of 1523 K for normal operation. The maximum temperature during a LOFC remains well below the generally accepted limit of 1873 K and the maximum fluence levels stay below the limit 8.0×10^{21} cm^{-2}.

However, the destruction capability for the LLFP in the DB-MODULE reactor is limited. Only Tc-99 seems to be effectively reduced. To achieve significant reduction of the LLFP or just compensation of their generation by fission events within the fuel particles, which is around 0.18 g per pebble, would require a high loading, which in turn reduces the achievable discharge burnup. This seems to negate any justification for the use of LLFP in the pebbles of an HTR-MODULE reactor, especially when taking into account the increase in expense on fuel fabrication, which is most likely to occur. Only the addition of Tc-99, which can be effectively reduced and in addition causes an improvement in the temperature coefficient, should be investigated further.

- *Core analysis of a HTR-MODULE design loaded with Deep-Burn fuel and Americium targets.*

The effect of adding Am targets to the DB fuel is similar to what was observed when adding LLFP materials: the discharge burnup of the DB fuel decreases with increased loading of the secondary particle, which in this case contains Am only. Through the addition of Am targets effective reduction of Am can be achieved at the 'penalty' of a lower discharge burnup of the DB-fuel. (Section 5.)

- *Earthquake performance of DB PBR*

At the end of the last Fiscal Year, a study the performance of a DB-PBR under earthquake conditions was carried out. It was shown that the reactor safely shuts down, as had been previously shown for a PBR fueled with UO_2. (See Appendix A-9 for details.)

7.2 CONCLUSIONS REGARDING THE ANALYSIS AND DESIGN OF THE DEEP-BURN COATED PARTICLE FUEL

- *Investigation of the impact of CO production and oxygen getter on the particle performance*

Recently published data of CO production in Pu-fuel has been implemented in the PASTA stress analysis code. The data predicts a minimal contribution of CO to the internal pressure of the coated particle with a negligible impact on the SiC stress during normal operation. However, it is noted that for higher temperatures and burnup levels a significant contribution of CO to the pressure is to be expected. The latter could be experienced during transients. Therefore, the use of an oxygen getter is still recommended. (Section 1 and Appendix A-8)

- *Investigation of the impact of the variation in the thickness of the particle coatings and the pebble core location on the performance*

The impact of the variation in coating thicknesses and of the location of the pebble in the core on the fuel performance was investigated. A statistical analysis that takes into account the variation of the buffer layer and the SiC layer thickness was performed. It revealed that particles that have both a small buffer and a thin SiC layer have a high probability to fail. However, the probability of this combination is small and therefore such a failure scenario does not contribute significantly to the average failure rate of a batch of particles. (See Appendix A-6.)

The radial location of the pebble within the core showed small variations in the corresponding coating stress level. A maximum variation of $\Delta\sigma = 25$ MPa was observed. This does not lead to a significant increase in the particle failure fraction as compared to using the radial average pebble temperature, since the SiC layer remains under low tensile stress levels. (See Appendix A-6.)

- *Transient analysis of the fuel performance during a Loss of Forced Cooling incident*

During a Loss Of Forced Cooling event in the reactor the fuel temperatures in some core regions are considerable higher than during normal operation. This results in an increase of the coating stresses and resulting particle failure. The failure fraction for Pu-only and Pu+MA fuels was 2.6×10^{-4} and 9.4×10^{-7}, respectively. (Details can be found in Section 3.2 and Appendices A-4, A-5.2, and A-7.)

- *Inter-comparison of fuel performance codes fuel coated particle stress analysis*

The PASTA code has been used extensively in this study. Although the code has been verified in the past against cases where analytical solutions are known, a full-fledged Verification and Validation process has not been implemented. However, a large measure of confidence can be reached in code-to-code comparisons between PASTA and other, independently developed, codes. The results produced by PASTA and the codes COPA and PISA were compared codes were compared for the analysis of a DB coated particle design that includes an oxygen getter. All three codes predicted no significant through-coating failure. The stress results were found to be sensitive to the dimensional change and creep of the PyC layers. (See Appendix A-8.)

8. APPENDICES: DETAILS OF STUDIES

This section presents a set of appendices that provide details of the various studies carried out in the course of this project and referred to in the body of the report. The Appendices are labeled A-1 to A-9.

A-1. CORE ANALYSIS AND OPTIMIZATION OF THE DEEP-BURN PEBBLE-BED REACTOR

In a FY 2009 analysis, the performance of the reference DB pebble-bed reactor (PBMR-400) was computed. A schematic overview of the reactor design and its nominal flux, power, and fuel temperature profiles are given in Figure 14.

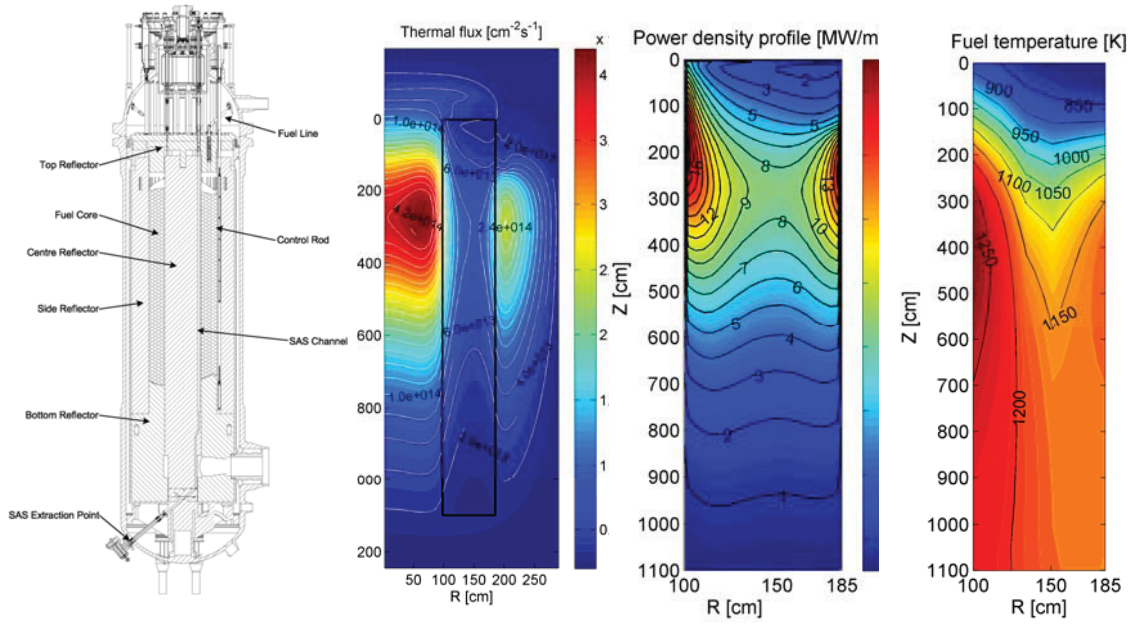

(a) (b) (c) (d)

Figure 14. (a) The PBMR-400 core design, (b) the thermal flux profile, (c) the power profile; and (d) the fuel temperature profile in the DB core. Thermal flux peaking near the inner and outer reflector results in power density and temperature peaking.

Figure 14(b) shows the thermal flux profile in the Pu-fueled (equilibrium) core. The peaks in the thermal flux profile in the inner and outer reflector result in peaks in the power density profile (Figure 14[c]) and fuel temperature (Figure 14[d]) near the reflector edges. Note that the maximum core temperature (1284 K) is located below the power peak of 17.7 MW/m^3 near the inner reflector, since the coolant flow direction is downward. Note that the temperature of an individual pebble with a low fuel burnup in this region of the core can exhibit higher temperatures (1541 K) than the average pebble.

For Pu and Pu + minor actinide (MA)-fueled pebbles reactor designs, it was found that the moderator temperature coefficient (MTC) is positive for low temperatures (T < 800 K) and high burnup values (B > 300 MWd/kg Heavy Metal [HM]). Since the fuel temperature coefficient (FTC) is small over the

entire range of temperatures and burnup values, the uniform temperature coefficient (UTC) is dictated by the MTC.

The following sections present the core optimization studies performed to improve the temperature coefficient (Appendix Section A-2) and to reduce the power and temperature peaking (Appendix Section A-3).

A-2. IMPROVEMENT OF THE TEMPERATURE COEFFICIENT

A-2.1 DESCRIPTION OF THE METHODOLOGY FOR ANALYZING THE TEMPERATURE COEFFICIENTS

A scoping study has been performed in which the temperature coefficient was calculated for several fuel loadings per pebble and for several Erbium concentrations in the kernel. A fixed temperature of 500 K has been used as well as a fixed nuclide composition set as a function the fuel burnup. For the most promising cases detailed full core coupled neutronics, thermal-hydraulics, and depletion calculations have been performed. The zone average nuclide compositions from these latter calculations have been used to calculate the temperature coefficient as a function of the core position and the temperature.

Er-167 has a large resonance at 0.5 eV, near the Pu-239 and Pu-241 resonances at 0.3 eV (Figure 15), which are important during a spectral shift, in addition to the increased absorption in the resonances with increasing temperatures (Doppler effect). The addition of Erbium to the fuel can therefore lead to an improvement of the moderator temperature coefficient.

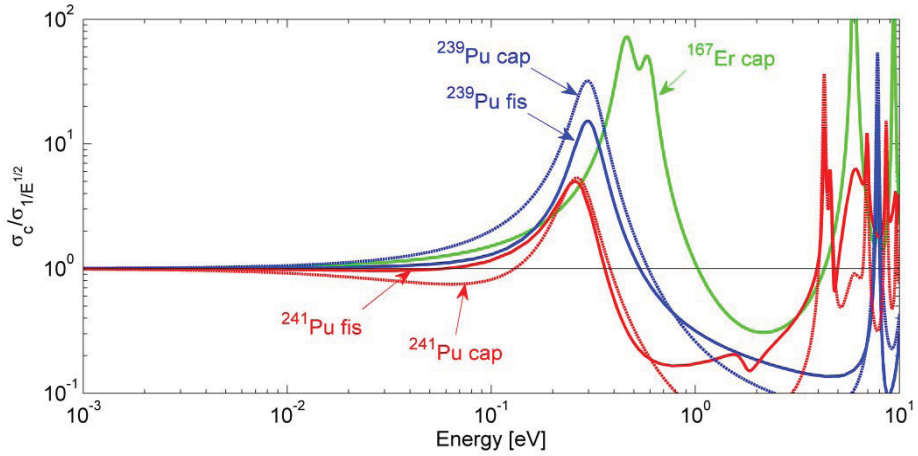

Figure 15. Capture and fission sections of Pu-239 and Pu-241and the capture cross section of Er-167 (normalized to their $E^{1/2}$ limit). The location of the Er-167 resonance near the resonances of the Pu isotopes results reduces the positive reactivity effect of a spectrum shift to higher energies.

A-2.2 RESULTS ON THE IMPROVEMENT OF THE TEMPERATURE COEFFICIENT

In practice, the core of a pebble bed reactor is a mix of pebbles with different burnup levels, which results from the recirculation of the pebbles. Normally the zones with the highest burnup value can be found near the (inner) reflector at the bottom of the core, since the pebbles move down with time (burnup) and the

highest thermal flux levels in the pebble bed are found near the inner reflector. The PEBBED, THERMIX, and SCALE-6 codes have been used to calculate the average nuclide densities, which represent the mixture of pebbles having different burnup levels, for several core zones. These nuclide densities are used to calculate the temperature coefficients as a function of the axial core position in a procedure similar to the one used in the body of the report. Figure 16 shows the UTC for several axial positions as a function of the temperature. It can be seen that at low temperatures (T < 800 K) a significant portion (75%) of the core has a positive UTC.

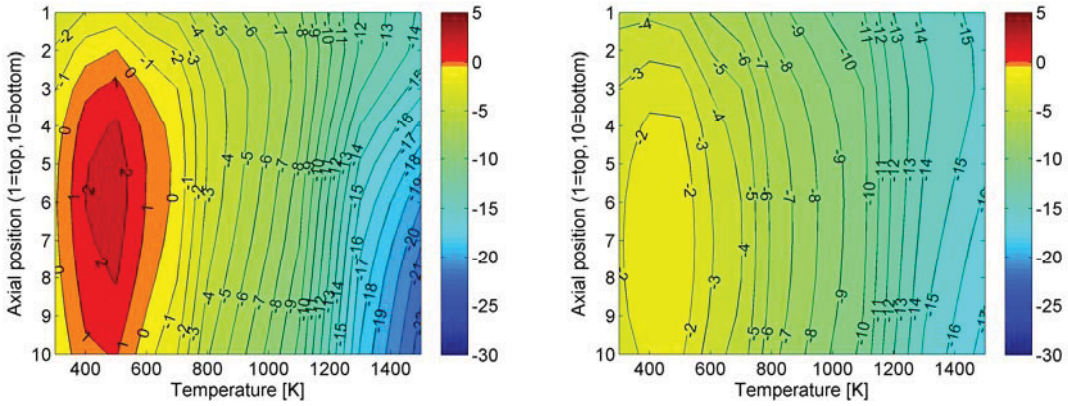

(a) (b)

Figure 16. Uniform Temperature Coefficients of reactivity in the Deep-Burn (Pu-fueled) PBMR as a function of the axial core position and the temperature; for the reference case without addition of Er (a) the core has a positive UTC at low temperatures at the bottom region; (b) a core-wide negative UTC is found for the entire temperature range for a case in which Er-167 was added at a density of 2.0×10^{-6} $(b.cm)^{-1}$ to the fuel kernel.

Table 10 shows the key results of the full-core parametric study in which the HM loading was varied between 2 and 3 g per pebble and the Er-167 density in the kernel between 0 and 2.0×10^{-6} $(b.cm)^{-1}$. The first two cases represent the reference core and fuel design for the two DB fuel types (with and without MAs). It is noted that for the reference case with initial MA in the fuel the maximum UTC in the core is lower when compared to the Pu-only fuel. This is the result of the lower discharge burnup in the Pu + MA-fueled core.

For the last three cases presented in the table, a cylindrical core concept (Section A-3) was adopted with the improved coated particle design of Section A-8.

It can be seen that by either increasing the HM load or by adding more Erbium the UTC decreases and can be made negative for the entire temperature range. This is in agreement with the simplified cases investigated in the previous sections.

The drawback of increasing the HM load is that the fast fluence attained by the pebbles increases. Experience with TRISO fuel for fast fluence levels above 8×10^{21} n/cm^2 is lacking and, therefore, makes this option unattractive. A loading of 3 g per pebble without burnable poison would get close to attaining this fluence level. On the other hand, increasing the Er-167concentration reduces the pebble discharge burnup and the Pu destruction capability of the reactor.

The temperature coefficient can be improved by addition of Er-167 and/or increasing the HM load per pebble without significantly sacrificing the pebble discharge burnup. The present analysis suggests that increasing the HM load from 2 to 3 g per pebble without burnable poison addition is the most attractive

option with regards to the achievable burnup. This option would keep the discharge burnup at 690 MWd/kg, while keeping the maximum UTC below -1 pcm/K. It is noted, however, that high fast fluence levels will be attained $\Gamma > 7.0\ 10^{21}$ cm^{-2} (E > 0.1 MeV) for loadings larger than 2.5–3g per pebble. It is unclear whether material integrity can be maintained for these fluence levels. Furthermore, the higher initial fuel loading per pebble will also result in a higher amount of residual minor actinides per pebble at the end of irradiation. As a result, this can lead to an increased decay heat level per pebble.

Table 10. Key results of the optimization of the DB pebble bed core for several HM land Er-167 loadings and fuel types.

Case	Fuel Type	HM Loading [g/pebble]	Er-167 kernel density [(b.cm)$^{-1}$]	Discharge burnup [MWd/kg]	Core maximum temperature [K]	Discharge fluence E > 0.1MeV [10^{21} cm^{-2}]	Core maximum UTC [pcm/K]
1	Pu + MA	2	0	505	1335	3.51	+0.70
2	Pu	2	0	687	1284	4.90	+2.58
3	Pu	2	1.0×10^{-6}	669	1272	4.76	+1.26
4	Pu	2	2.0×10^{-6}	620	1299	4.38	-1.20
5	Pu	2	2.5×10^{-6}	525	1340	3.62	-2.76
6	Pu	3	0	690	1285	7.23	-1.43
7	Pu	3	1.0×10^{-6}	660	1308	6.81	-2.72
8	Pu	3	2.0×10^{-6}	600	1339	6.02	-3.68
9	$MAO_{1.8}(SiC)_{0.6}$*	2	0	567	1189	4.45	-0.74
10	$MAO_{1.8}(SiC)_{0.6}$	2	0.5×10^{-6}	487	1259	3.79	-2.22
11	$MAO_{1.8}(SiC)_{0.6}$	2	0.7×10^{-6}	457	1280	3.56	-2.54

*See Table 16 and Table 17 for fuel type specifications.

One can also choose to add Erbium to the pebbles to improve the temperature coefficient. A penalty of ~100 MWd/kg on the achievable burnup has to be paid to ensure a negative temperature coefficient for the entire core and temperature domain. From the previous sections it was found that the Erbium can possibly made more effective by using separate particles or by locating the Erbium at the very center of the coated fuel particles or using it in separate particles.

Erbium is depleted as the pebbles move downward in the pebble bed core. As a result, the power peak shifts downward with increased Erbium loading, since a higher concentration of the (Erbium) absorber material is located at the top of the core. For the reference case (without Erbium) the power peak matches the axial fluid temperature profile, resulting in a relatively flat fuel temperature profile. With the power peak shifted downward, higher fuel temperatures are encountered as can be observed in Table 10. The maximum fuel temperature can probably be reduced for these cases by reducing the total number of pebble (re)circulations. However, this would probably in turn increase the maximum UTC in the core, since the Erbium is less effective at the core bottom region, where it is needed most.

A-3. REDUCTION OF THE POWER AND TEMPERATURE PEAKING IN THE CORE

This section presents the studies aimed at a reduction of the power peaking in the DB pebble bed core. Peaks are ordinarily present near the inner and outer reflectors. A scoping study (in which the geometry and material composition of the core is varied) has been performed first. This analysis uses a 1-D

transport calculation (XSDRNPM code), which represents a radial slice of the core and the reflector(s). This study was followed by a full core calculation for the most promising concepts.

The following parameters were varied in the preliminary scoping study:

1. The outer radius of the pebble bed in a cylindrical core design
2. The outer radius of the inner reflector
3. The graphite density of the inner reflector
4. The number of graphite-only pebbles in the pebble bed
5. Beryllium carbide (Be_2C) at various concentrations as a secondary moderator material.

The optimal power (thermal flux) profile would be a radial flat one during normal operations, resulting in a radially flat temperature distribution (assuming uniform heat convection throughout the core). For a depressurized LOFC incident in which the heat is transported by conduction and radiation to the outer surface of the reactor, a profile with a peak at the outer rim of the core is optimal.

A-3.1 CONCLUSION ON THE POWER PEAKING REDUCTION

From the scoping studies presented in the previous sections, two cases were selected and further investigated with a full core analysis with PEBBED-THERMIX-SCALE: a reduced center reflector; and a cylindrical core design. Key results are presented in Table 11.

The effect of the reduced inner reflector graphite density and a cylindrical core design on the power peak is shown in Figure 17 (a) and (b), respectively. It can be seen that for a low graphite density ($\rho = 0.05\rho_0$) the inner peak in the thermal flux completely disappears and that the power peak also vanishes (Figure 17 [a]). The power peak in the core, which is now located near the outer reflector, is 12.1 MW/m^3. As a result the maximum temperature during an LOFC transient reduces from 2072 K to 1871 K. Furthermore, the maximum fuel temperature that a given pebble experiences during its lifetime decreases from 1541 K to 1301 K.

As an alternative to the annular core with a transparent inner reflector, a cylindrical core design is adopted in this section in an attempt to avoid power (and temperature) peaking in the inner and outer core region. The proposed design is based on the HTR-PM design (Figure 18 [a]), which has a pebble bed core diameter of 3 m, a height of 11 m, and a thermal power of 250 MW. Compared to the PBMR-400 design, the helium coolant inlet and outlet temperature have been lowered to 250°C and 750°C, respectively, and the number of pebble passes is increased from 6 to 20. For further details of the design and material properties see Zheng et al.'s article [13].

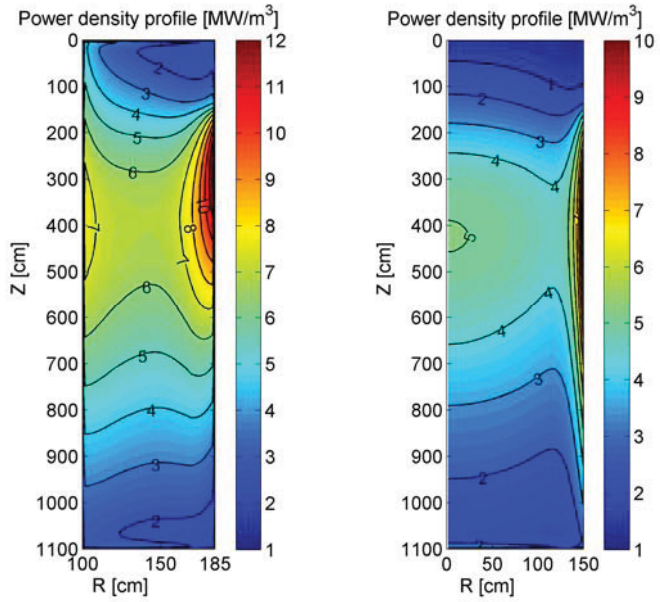

(a) (b)

Figure 17. (a) Power density profile of an annular core with reduced inner reflector density ($\rho = 0.05\rho_0$) and (b) the profile in the DB HTR-PM (cylindrical) design with 20 pebble circulations.

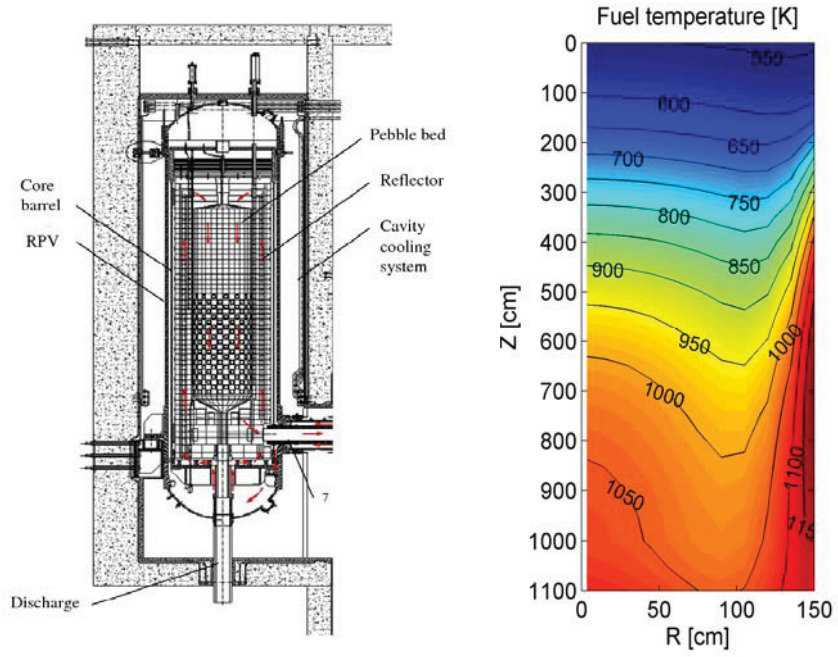

(a) (b)

Figure 18. (a) The 250 MW_{th} cylindrical HTR-PM design [13] and (b) the temperature profile (pebble center) for a DB fuel loaded core.

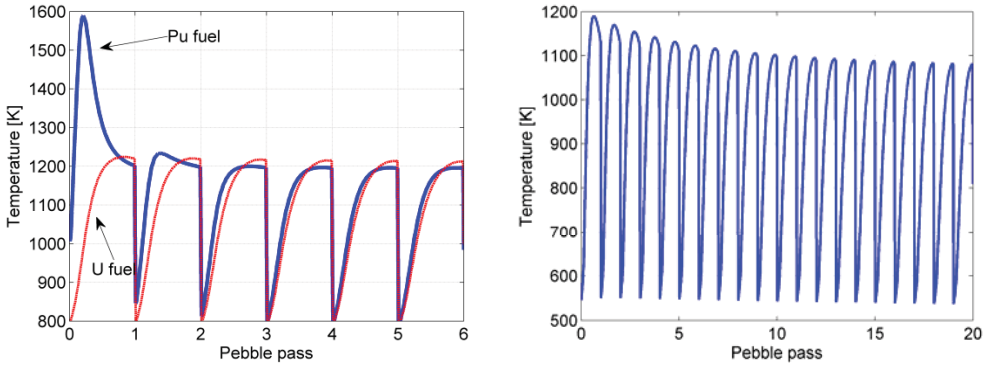

(a) (b)

Figure 19. (a) The temperature history of a pebble in the PBMR-400 for both UO_2 fuel and Deep-Burn fuel (6 pebble circulations); and (b) the temperature history in the DB fueled HTR-PM design (20 pebble circulations).

The power density profile of the DB HTR-PM design is shown in Figure 17(b). It can be seen that the power profile is flattened in the radial direction as compared to the power profile of the annular core (Table 11), while a higher discharge burnup of 567 MWd/kg is achieved. The power peak at the core center, where the maximum temperature occurs, is reduced from 17.7 MW/m^3 to 10.8 MW/m^3. The power profile is flattened in the axial direction as a result of the increased pebble in-core (re)circulation (increased from 6 to 20).

Compared to that of the reference design, the core maximum temperature at nominal conditions is reduced from 1335 K to 1189 K (Figure 18). The maximum fuel temperature during the first pebble pass is reduced from 1406 K to 1190 K (Figure 19), and the maximum fuel temperature during a DLOFC transient is reduced from 1961 K to 1734 K. It is noted that these temperatures are calculated using a conservative graphite thermal conductivity, which is fixed at a value of 26 W/m/K. The maximum temperature in a cylindrical design during a LOFC, which is also know as a conduction cool-down event, is sensitive to this conductivity. If a temperature dependent (best-estimate) conductivity based on German data is used, the temperature peak is expected to be 50 K lower [13] (see Section A-5).

Table 11. Key results of the optimization of the DB pebble bed core with respect to the maximum power and temperature for several HM core and fuel types.

Case	Fuel Type	Core Type	Norm. Reflector Density	Discharge Burnup [MWd/kg]	T core max. [K]	T Pebble Peak [K]	q''' core [MW/m^3]	q Pebble Peak [kW]	T DLOFC max. [K]
1	Pu+MA	Annular	1.0	505	1335	1406	20.8	3.07	1961
2	Pu	Annular	1.0	687	1284	1541	17.7	6.03	2072
3	Pu	Annular	0.05	700	1272	1301	12.1	4.28	1871
4	Pu	Annular	0.10	699	1299	1311	11.8	4.72	1910
5	Pu	Annular	0.20	699	1340	1493	13.8	7.23	2101
6	$MAO_{1.8}(SiC)_{0.6}$*	Cylinder	N/A	567	1189	1190	10.8	2.35	1734

*See Table 16 and Table 17 for fuel type specifications.

A-3.2 PRELIMINARY RESULTS OF USING MIXED MODERATORS TO LOWER PEAKING

It is intuitive that the introduction and use of beryllium carbide (Be_2C) alongside graphite (or other forms of carbon) has the potential of resulting in spectral shifts within the reactor. Such spectral shifts may be exploited to lower peaking and to improve reactivity coefficients. This section presents results obtained by introducing various amounts of Be_2C into the fuel pebbles or dummy Be_2C pebbles into the core zone or into reflectors. The results shown here are preliminary in nature because they are based on free gas data, as the S(α,β) for Be_2C were not available at the time the study was conducted.

Be_2C has a smaller diffusion length than graphite ($L_{T,Be}$ = 21 cm, $L_{T,C}$= 59 cm). This changes the spectrum in the pebble bed and modifies the flux profile, i.e. the thermal peaks in the reflectors are reduced. Figure 20 shows the effect of Be_2C on the radial flux profile, indicating that the profile flattens with increasing Be_2C concentration in the pebbles. Figure 21 shows the effect on the power peak in the DB pebble bed reactor of gradually replacing the graphite in the pebbles by Be_2C. The black line shows the point where the entire graphite matrix (inner 2.5 cm fuel zone) has been replaced by Be_2C. At higher Be_2C volume percentages part of the graphite shell also is replaced by Be_2C. A maximum reduction of the power peak with 14 %, from 1.98 to 1.71 is achieved when the entire pebble uses Be_2C instead of graphite as the moderator. Figure 22shows the effect in a cylindrical core of placing Be_2C in the pebbles and/or outer reflector.

Finally, Table 12 shows the effect of the Be_2C addition on the reactivity coefficients, which display a significant improvement over the no Be_2C base case. These latter results must be considered with great caution, as the thermal scattering was not properly treated in this study since the relevant S(α,β) data were not yet available.

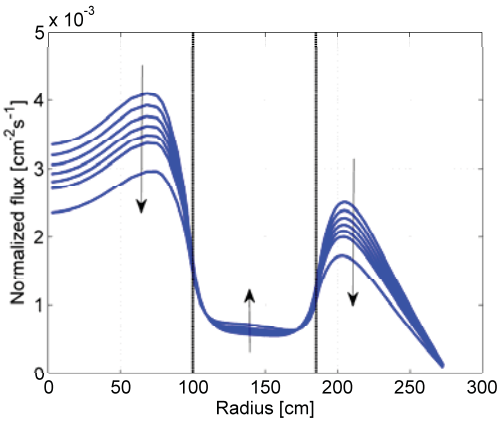

Figure 20: Effect of the volume percentage of Be_2C in a pebble on the thermal flux shape in the core. The arrows show the direction of increasing Be_2C volume percentage, i.e. the flux profile flattening effect.

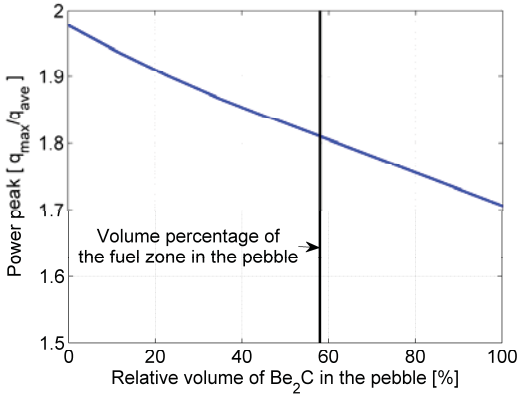

Figure 21: Power peak (normalized to the average power) in an annular core as a function of the volume percentage of Be_2C in a pebble.

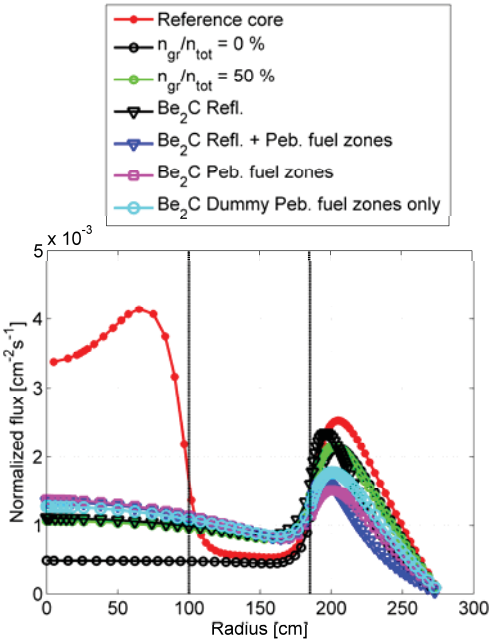

Figure 22: Thermal flux profile (radial) in a cylindrical pebble bed reactor showing the impact on the flux shape for Be_2C at different locations in the core, such as the inner zones of the 'dummy' and fuel pebbles.

Table 12: Temperature reactivity coefficients for the fuel (FTC), moderator (MTC) and the uniform (UTC) temperature with the Be_2C location as a parameter (assuming n_{dummy}/n_{tot} = 50 %).

Location	FTC	MTC	UTC
Outer Reflector	-0.84	-4.25	-5.10
Fuel zone of dummy and fuel pebbles	-0.84	-4.27	-5.13
Fuel zone of dummy pebbles	-1.03	-4.57	-5.62

A-4. ANALYSIS OF THE DECAY HEAT OF DEEP-BURN FUEL

The decay heat of DB fuel is expected to be different in magnitude from that of 'standard' UO_2 fuel. The decay of fission products and unstable minor actinides is mainly responsible for the decay heat in used fuel. The inventory distribution of fission products is expected to be slightly different in DB fuel than what it is on UO_2 fuel. Furthermore, DB fuel consists of Pu with possible addition of minor actinides. This reduces the time lapse from initial fueling and irradiation to the production of unstable minor actinides. Their contribution to the decay heat can therefore be considerable in DB fuel.

A-4.1 COMPARISON OF DECAY HEAT CURVES OF UO_2, PU AND PU+MA FUELS

The decay heat curves of the different fuel types are compared with each other in Figure 23 through Figure 25. From Figure 23 it can be seen that the decay of Pu fuel is lower for the average burnup fuel, but higher for the discharge burnup level fuel when compared to UO_2. This is also true for the case when Pu + MA fuel is compared with UO_2 (Figure 24). The decay heat of Pu + MA fuel at discharge level is however considerably lower than that of the Pu fuel (see Figure 25). This is the result of the lower discharge burnup level of the Pu + MA fuel (600 MWd/kg compared to 700 MWd/kg of the Pu + MA).

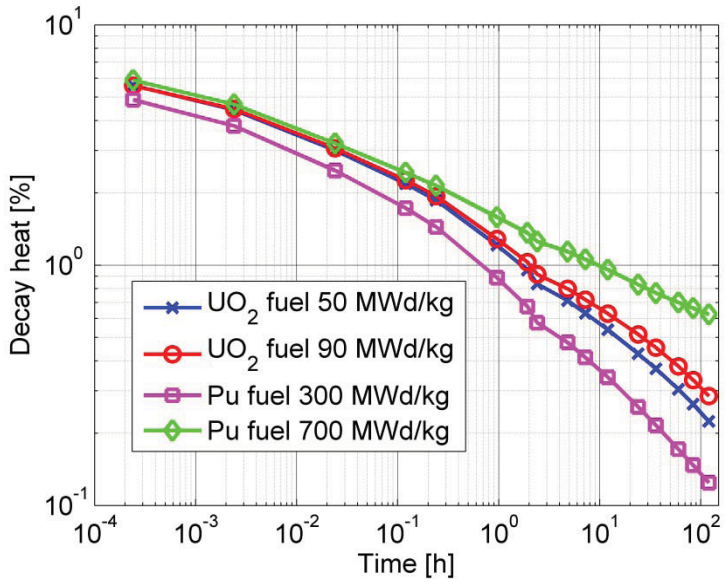

Figure 23. Comparison of the decay heat of UO_2 and Pu fuel at the an average burnup (50 MWd/kg for UO_2, 300 MWd/kg for Pu fuel) and the discharge burnup (90 MWd/kg for UO_2, 700 MWd/kg for Pu fuel).

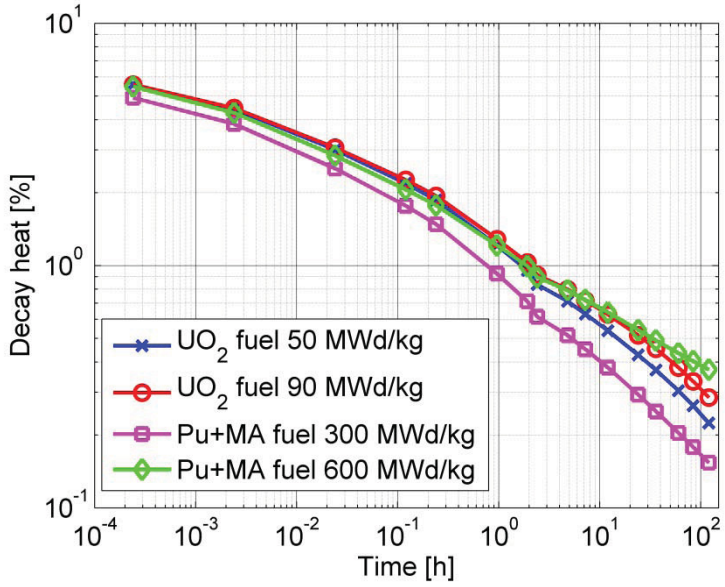

Figure 24. Comparison of the decay heat of UO_2 and Pu + MA fuel at the average burnup (50 MWd/kg for UO_2, 300 MWd/kg for Pu fuel) and the discharge burnup (90 MWd/kg for UO_2, 600 MWd/kg for Pu+MA fuel).

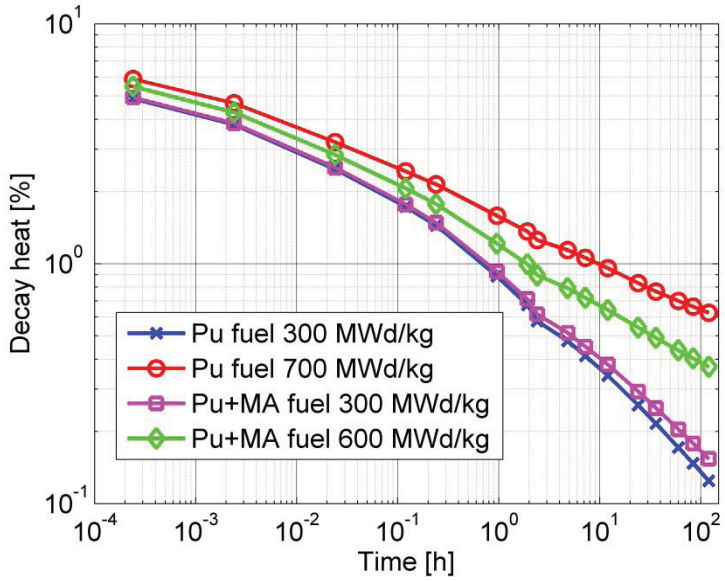

Figure 25. Comparison of the decay heat of Pu and Pu+MA fuel at the average burnup (300 MWd/kg for Pu fuel) and the discharge burnup (700 MWd/kg for Pu, 600 MWd/kg for Pu+MA fuel).

The following conclusions can be drawn:

1. The decay heat curve of DB fuel is similar to but slightly lower than that of standard UO_2 fuel at low burnup levels.

2. The decay heat curve of the DB fuel at high burnup levels B > 600 MWd/kg is significantly influenced by the contribution of the unstable MAs. These nuclides give a relatively large contribution for these burnup levels, especially after several hours of decay (t > 2 hours).
3. The decay heat curves of the two DB fuels considered in this study are very similar. Because the Pu only fuel is able to attain a higher discharge burnup level, the decay heat is also higher for this fuel type.

A-5. ANALYSIS OF THE DB HTR-PM UNDER DLOFC TRANSIENT CONDITIONS

From the previous section, it is seen that the decay heat curves of DB fuel display a significantly higher power output for high burnup levels after several hours of decay, when compared to standard UO_2 fuel. Furthermore, the fast fluence level attained in the DB pebbles is expected to be twice as high as in UO_2 fuel ($\Gamma > 6 \times 1021$ [E > 0.1 MeV]), which could result in a significant reduction in the thermal conductivity of the graphite and in the effective conductivity of the pebble bed.

Both effects described above can result in higher (fuel) temperatures during a (depressurized) LOFC incident. The impact of the above effects has been investigated for the Chinese cylindrical HTR-PM design [14]. It was expected that this design would provide sufficient margin in the temperature limits for the fuel and metal structures, based on the analysis of Zheng et al. [13].

A model of the HTR-PM has been constructed for for the PEBBED-THERMIX code and the equilibrium core has been modeled and evaluated.

A-5.1 RESULTS FOR THE HTR-PM CORE UNDER NORMAL OPERATION

The equilibrium core composition has been calculated with PEBBED for the DB HTR-PM and the power density profile (Figure 26a) was determined (Pu-fueled core with 15 pebble [re]circulations). The profile power is similar to the one for the UO_2 fueled core [13] with two power peaks at the core center and outer rim, at an axial height of Z = 300 cm. The maximum power at the core center is 8.1 MW/m^3, which is higher than for the UO_2 fueled core (6.6 MW/m^3). The resulting temperatures of the solid structures in the reactor are shown in Figure 26(b) and the pebble center temperatures in the core are shown in Figure 27. The highest temperatures occur at the core radial center in the bottom region as a result of the center power peak and the downward flow. The maximum pebble center temperature (860°C) is located at Z = 675 cm, while the UO_2 core has a maximum value of 890°C [13]. The average fuel temperature is 600°C for the DB and the UO_2 cores.

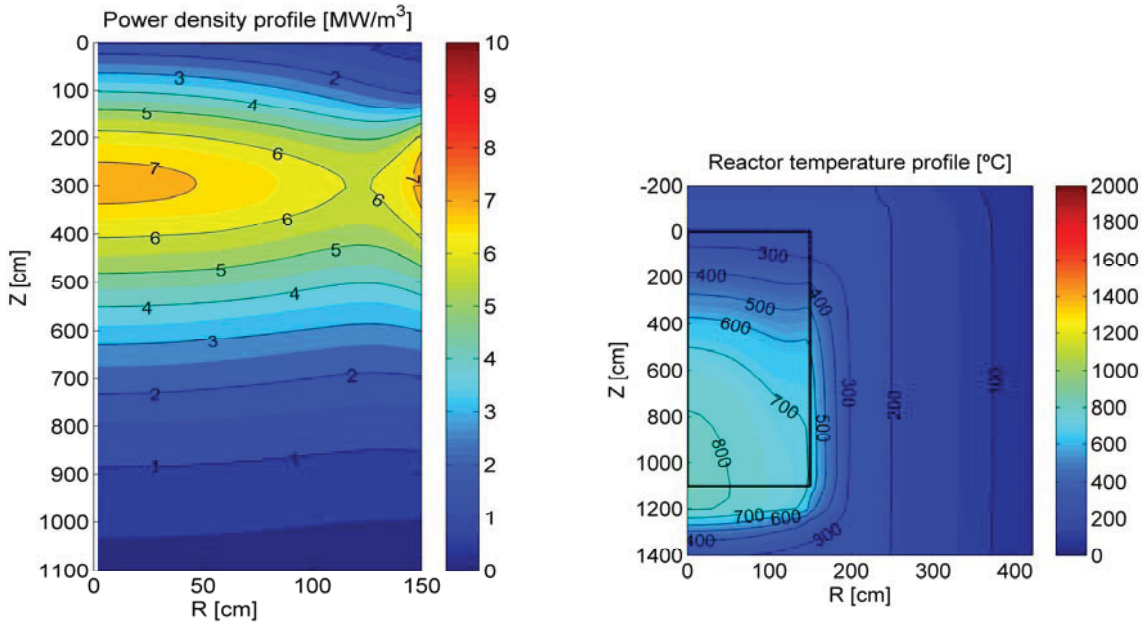

(a) (b)

Figure 26. (a) Power density profile in the DB pebble bed core (Pu fuel, 15 pebble circulations); and (b) the temperature profile for the entire DB HTR-PM reactor.

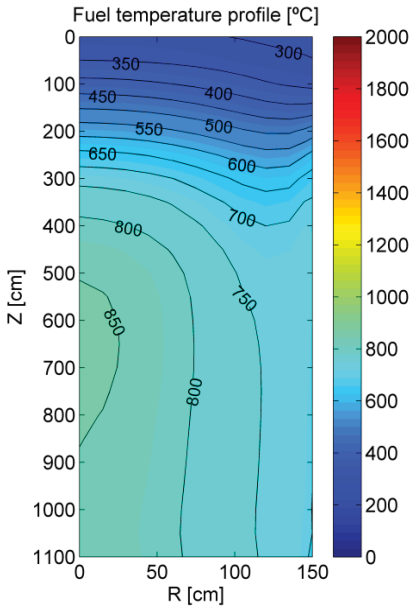

Figure 27. Profile of the pebble center temperatures in the core at the start of the transient. The maximum pebble center temperature in the core is 860°C.

The peak temperatures of the reactor pressure vessel (RPV) and the core barrel (CB) during normal operation 150°C and 179°C, respectively. These temperatures are significantly below the value of 250°C for both the RPV and the CB found for in Zheng et al.'s article [13]. This reference explicitly considers

the part of the RPV and the CB, where the helium coolant enters the core a temperature of 250°C. This part is not represented explicitly in the INL model.

A-5.2 RESULTS OF THE CORE DURING A DLOFC AND CODE-TO-CODE COMPARISON

A transient calculation using the THERMIX code has been performed. It is assumed that the reactor depressurizes instantaneously from 7 MPa to 0.1 MPa and that the coolant mass flow is reduced to zero at the same time. Assuming a reactor SCRAM, the power is determined by the decay only. The standard decay heat curve that is supplied by THERMIX (Figure 28) is assumed first and results are compared with the results in Zheng et al.'s article [13]. A decay heat curve specific for DB fuel is implemented in THERMIX and the impact on the core temperatures is evaluated. Furthermore, the influence of the higher fast neutron dose level of the DB pebbles on the temperature is evaluated.

After initiation of the transient, the core starts to heat up from deposition of the decay heat in the absence of forced cooling. Figure 29(a) shows the average and peak fuel temperatures in the core during the transient. Heat from the core is transferred to the reactor heat removal system (RHRS) that surrounds the RPV from a distance of 1 m. These water panels are assumed to be at a constant temperature of 70°C. Heat from the pebble bed core is transferred by conduction and thermal radiation to the side reflector. Heat is conducted through the reflector and the RPV, where thermal radiation effectively transfers the heat to the RHRS. The temperature histories of the RPV and CB are shown in Figure 30(a) and the heat load of the RHRS is given in Figure 30(b).

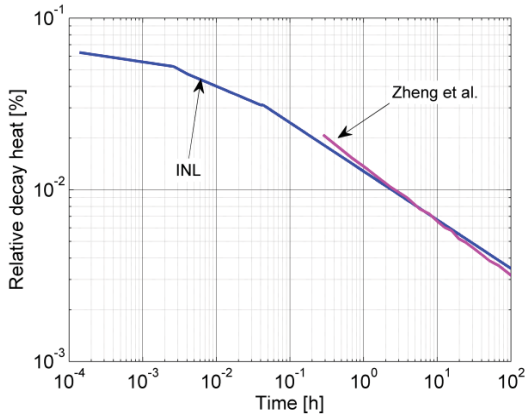

Figure 28. Decay heat curves used in the INL model and in Zheng et al [13].

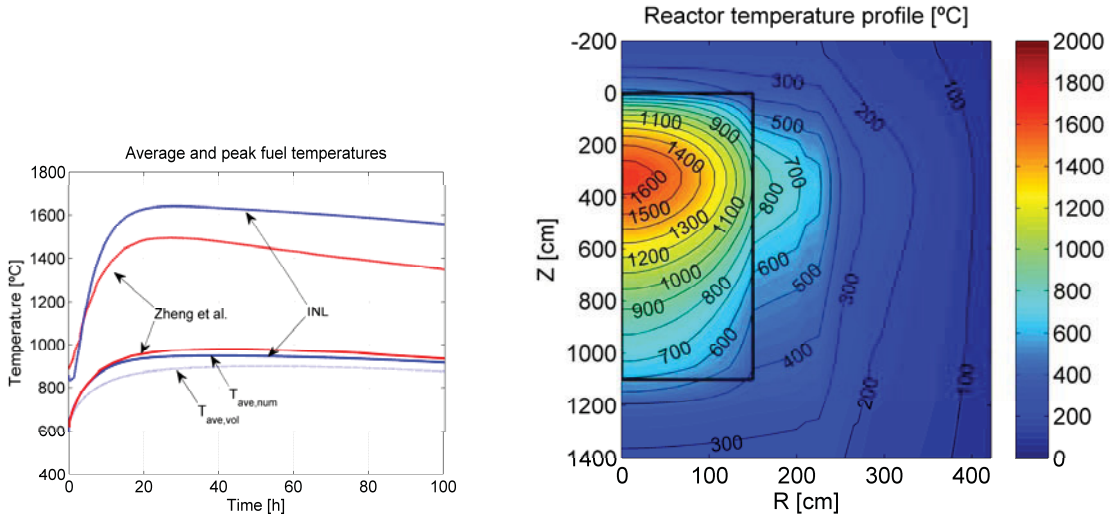

(a) (b)

Figure 29. (a) Maximum (dashed line) and average (solid line) fuel temperature during the DLOFC transient for both INL and Zheng et al. results; and (b) the temperature profile for the entire DB HTR-PM reactor at the time point of the maximum fuel temperature.

After the initial temperature rise, the core starts to cool down at the point where the decay heat equals the amount of heat transferred to the RHRS. After 27.5 hours, the core reaches a maximum core peak temperature of 1639°C. Figure 29(b) shows the temperature profile in the reactor. The figure shows that only a small part of the core is at this high temperature. This is also reflected in the volume weighted average core temperature, which reaches a maximum value of only 897°C after 52.6 hours.

The data and results by Zheng et al. [13] for the UO_2 fueled HTR-PM have been shown in Figure 28 through Figure 30. Although the trends are similar to those of the DB HTR-PM of INL, some differences can be identified. The maximum fuel temperature in the core is significantly higher in the INL analysis. It can be seen that the decay heat (Figure 28), the history of the average fuel temperature (Figure 29a) and the heat transferred from the reactor (Figure 30b) compare reasonably well. Therefore, the difference in peak fuel temperature is plausibly attributable to the difference in the power profile, which is relatively flat for the UO_2 case [13] compared to the DB case.

Figure 31 shows the radial temperature profile at the (axial) center of the core at t = 50 hours. The temperature profiles of the two results compare reasonably well except for the part close to the core center. From Zheng et al.'s article [13] it was found that the power density during normal operation at this position (Z=550 cm, R=0 cm) is around 4.5 MW/m^3, while the calculated power density of the DB core at this position is around 4.0 MW/m^3 (Figure 2a). This explains the lower temperature at this position in the DB core and indicates that the higher power peak (8.1 MW/m^3 compared to 6.6 MW/m^3) at Z=300 cm is responsible for the higher peak temperature at that position.

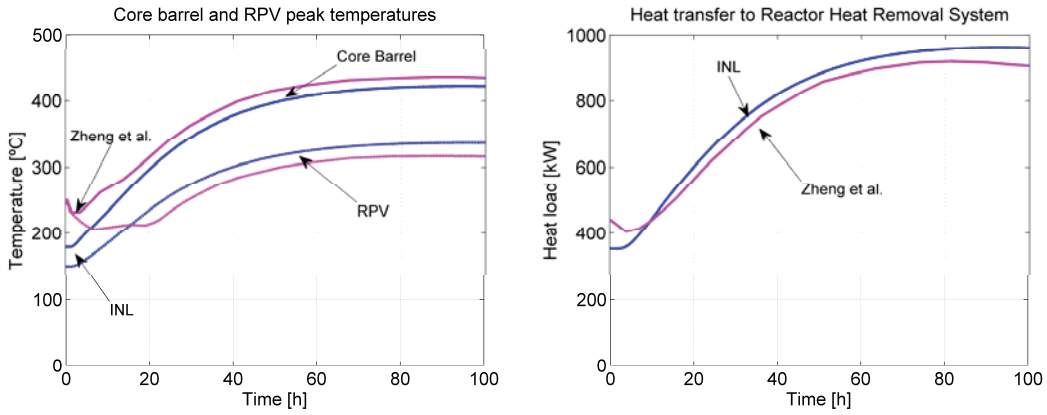

(a) (b)

Figure 30. (a) The peak temperature of the RPV and the CB during the DLOFC transient for both INL and Zheng et al. results; and (b) the heat load of the Reactor Heat Removal System.

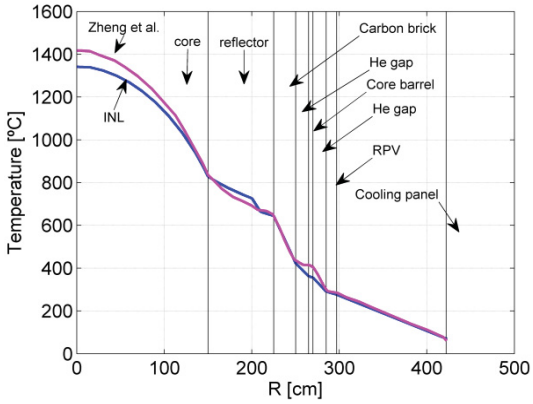

Figure 31. The radial temperature profile at the axial core center during the DLOFC transient at t=50 hours for both INL and Zheng et al.

A-5.3 IMPACT OF THE DEEP-BURN DECAY HEAT ON THE CORE TEMPERATURES

The impact of the decay heat curve on the maximum fuel temperature is investigated. A decay heat curve for DB fuel has been calculated using the ORIGEN-S code. The curve has been implemented into THERMIX. Figure 32 shows the two decay heat curves and Figure 33 shows the effect of using one or the other decay heat curve on the fuel temperature during the DLOFC transient. The DB decay heat is lower in the beginning of the transient, but higher for t > 5 hours. Therefore, both the average and peak fuel temperatures are lower in the beginning of the transient for the DB decay heat case. The maximum temperatures are higher and are reached at a later time in the transient (peak temperature of 1675°C at t = 69.4 hours). While the peak temperature reached is 90°C higher for the DB fuel than for the UO_2 decay heat curve, the core peak temperature is lower for the first 16 hours of the transient.

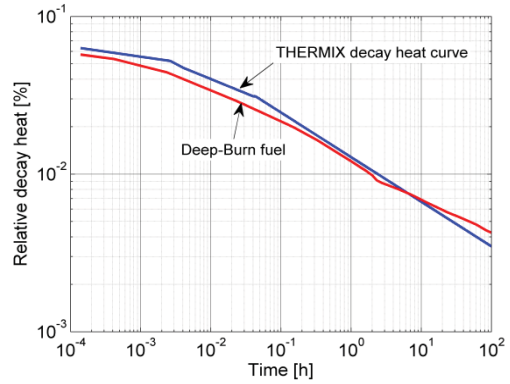

Figure 32. Decay heat curve provided in THERMIX and a decay heat curve calculated using ORIGEN-S for typical Deep-Burn fuel.

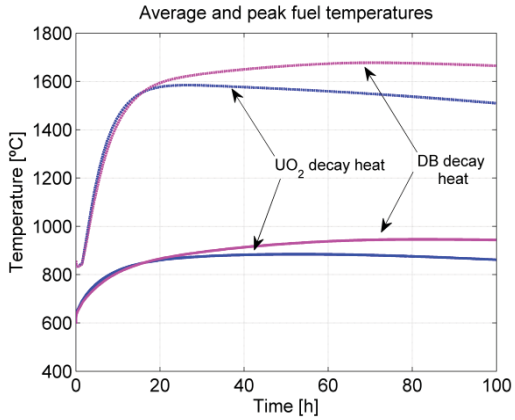

Figure 33. Effect of different decay heat curves (for UO_2 or Deep-Burn fuel) on the fuel average and peak temperatures during a DLOFC transient.

A-5.4 IMPACT OF THE INCREASED NEUTRON DOSE LEVEL ON THE CORE TEMPERATURES

The impact of the neutron dose on the maximum and average fuel temperatures, the maximum CB and the maximum RPV temperatures during the DLOFC transient have been investigated. Both the fast neutron dose levels of the pebbles and of the reflectors have been varied. Results are presented in Table 13. The maximum values of the peak and average core temperature increase significantly with increasing fast neutron dose level. Both the increase in the dose level of the pebbles and that of the reflector have a large effect on the fuel temperature.

The limit of the fast neutron dose level for the graphite reflectors is assumed to be around 3.0×10^{22} n/cm^2 (E> 0.1 MeV) [15], equivalent to 1.7×10^{22} n/cm^2 EDN.* The fast neutron flux (E> 0.1 MeV) in the reflector of the DB HTR-PM is shown in Figure 34. The fast flux peak (4.5×10^{13} cm^{-2}s^{-1}) in the side reflector is comparable to that of UO_2 fueled HTR designs, such as the PBMR-400. In this latter annular core design the inner reflector is planned to be replaced after 18 years of operation, which is equivalent to a dose level of 2.6×10^{22} n/cm^2 for the region of the peak. Figure 34

* "Equivalent DIDO Nickel" from the British DIDO (MTR) reactor, based on nickel activation flux determination (conversion factor: 1.7/3.0 from >0.1 MeV to EDN)

shows that only a small part of the reflector in the DB HTR-PM will attain these high dose levels. Only 25% of the reflector will attain a dose level above 5.0×10^{21} EDN during the lifetime of the reactor (60 years). Therefore Cases 8 and 9 of Table 13 can be seen as very conservative cases.

The time at which the maximum fuel temperature is reached is significantly delayed with increasing reflector dose. The heat transferred to the RHRS is reduced, because the conductivity of the reflector is lower for the high dose levels. The reduced heat transfer is also reflected in lower CB and RPV temperatures. Therefore, it takes longer before the amount of decay heat generated is lower than the amount of heat removed from the reactor. This leads to a longer time during which the core is heated up, i.e., its temperature rises. For Cases 7-9 in Table 13, the maximum peak fuel temperature has not been reached within the 100 hour-time domain of the calculation.

Table 13. Impact of the fast neutron dose level on core parameters for a DLOFC transient.

Case	Case description	$T_{peak,max}$	$t_{peak,max}$	$T_{ave.,max}$	$T_{CB,max}$	$T_{RPV,max}$
1	Reference case.	1639°C	27.5 h	889°C	422°C	337°C
2	Temperature dependent Zehner-Schlünder.	1585°C	26.5 h	885°C	422°C	337°C
3	Same as Case 2, but DB decay heat curve.	1677°C	70.5 h	946°C	449°C	356°C
4	Same as Case 3, but dose level of *pebbles* is 1.0×10^{21} EDN.	1712°C	66.5 h	968°C	450°C	357°C
5	Same as Case 3, but dose level of *pebbles* is 2.0×10^{21} EDN.	1718°C	66.5 h	973°C	450°C	358°C
6	Same as Case 3, but dose level of *pebbles* is 2.5×10^{21} EDN.	1719°C	66.5 h	974°C	450°C	358°C
7	Same as Case 6, but dose level of *reflector* is 5.0×10^{21} EDN.	1877°C	100 h	1143°C	444°C	353°C
8	Same as Case 6, but dose level of *reflector* is 15.0×10^{21} EDN.	1931°C	100 h	1185°C	435°C	347°C
9	Same as Case 6, but dose level of *reflector* is 30.0×10^{21} EDN.	1948°C	100 h	1200°C	433°C	344°C

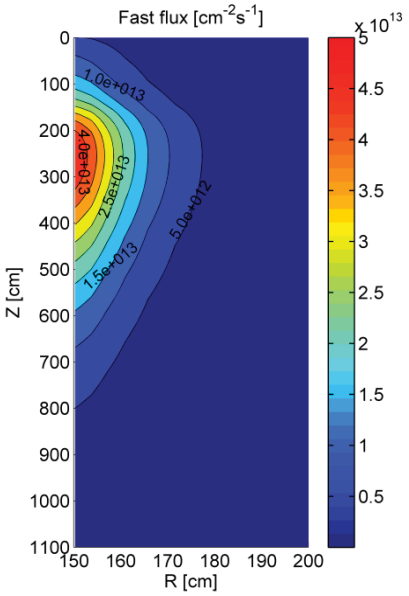

Figure 34. Fast neutron flux profile in the side reflector of the DB HTR-PM.

A-5.5 IMPACT OF A REDUCTION IN REACTOR POWER ON THE CORE TEMPERATURES

The reactor power of the DB HTR-PM has been varied in the DLOFC transient calculations to investigate the effect on the core temperatures. A fast neutron dose level of 2.5×10^{21} n/cm^2 EDN and 5.0×10^{22} n/cm^2 EDN for the pebbles and side reflector are assumed, respectively (Case 7 of Table 13). The decay heat curve for DB fuel was adopted. The helium mass flow has been kept constant for all cases.

Table 14 shows that the core peak and average temperatures are approximately linearly dependent of the reactor power. The peak temperature can be reduced to 1600°C, which is the generally accepted fuel temperature limit, when the reactor power is reduced to 192 MW. Since the mass flow is kept constant in this study, this reduction in reactor power would also result in a reduction of the helium outlet temperature to 634°C. This outlet temperature could be increased in turn to 750°C by reducing the mass flow without significantly increasing the maximum temperatures during the DLOFC transient.

Table 14. Impact of reactor power reduction on the core temperatures during a DLOFC transient.

Case	$P_{reactor}$	$T_{peak,max}$	$t_{peak,max}$	$T_{ave.,max}$	$T_{CB,max}$	$T_{RPV,max}$
1	250.0 MW_{th}	1877°C	100 h	1143°C	444°C	353°C
2	237.5 MW_{th}	1816°C	100 h	1105°C	435°C	346°C
3	225.0 MW_{th}	1756°C	99.5 h	1067°C	426°C	340°C
4	212.5 MW_{th}	1697°C	95.5 h	1030°C	417°C	332°C
5	200.0 MW_{th}	1638°C	82.5 h	993°C	406°C	324°C
6	187.5 MW_{th}	1581°C	79.5 h	956°C	396°C	316°C

A-5.6 CONCLUSION ON THE DB HTR-PM TRANSIENT ANALYSIS

The following conclusions can be drawn:

- The decay heat power of DB fuel is higher than that of UO_2 for the time domain t > 5 hours. As a result the maximum core peak and average temperatures during a DLOFC transient in the DB HTR-PM are higher (92°C versus 61°C in the UO_2 case). Also, the time at which these maximum temperatures occur is delayed by 44 hours.
- The maximum temperatures during a DLOFC are sensitive to both the neutron dose level of the pebbles and of the side reflector. For a best estimate value of the dose levels the maximum core peak temperature increases by an additional 200°C, to reach 1877°C. It is noted here that this increase is also to be expected for the standard HTR-PM with UO_2 fuel and was not taken into account in Zhang et al.'s article [13].
- The high temperatures during the DLOFC in the DB core can be reduced to 1607°C by reducing the reactor power from 250 MW to 192 MW, while retaining a helium outlet temperature of 750°C. A more attractive way to reduce the maximum temperature might be achieved by increasing the number of pebble recirculation passes.

A-6. FUEL PERFORMANCE ANALYSIS OF THE DEEP-BURN PEBBLE-BED REACTOR

A-6.1 INVESTIGATION OF THE IMPACT OF THE VARIATION IN THE PEBBLE LOCATION AND IN THE THICKNESSES OF THE PARTICLE COATINGS ON THE PERFORMANCE

The PASTA code has been further improved to allow for the evaluation of coating stresses during slow transients such as a LOFC incident in the Deep Burn Pebble Bed core (after the intial SCRAM). Furthermore, the code is now capable of treating the statistical variation in the coating thicknesses and calculating the coating stress as a function of the pebble position in the core.

The following sections show the stress is affected by the radial core position of the pebble and by the variation in the size of the coatings. Also shown is the influence of the free oxygen per fission. In Section A-7 the performance during the LOFC transient conditions is presented. (An overall conclusion on the performance of the two types of fuel investigated in this study and for the various cases is given in the body of the report in Section 4.3.)

A-6.2 SiC COATING STRESS AS A FUNCTION OF THE PEBBLE LOCATION

A fuel performance analysis is performed that takes into account the fuel temperature variation in the radial direction of the core. Figure 35 shows 2-D core distribution maps of the maximum SiC stress in the particles. The results show that the pebbles near the radial edges of the pebble bed, which experience high temperatures, contain particles that are subjected to a significantly higher SiC layer stress in comparison to the average particle.

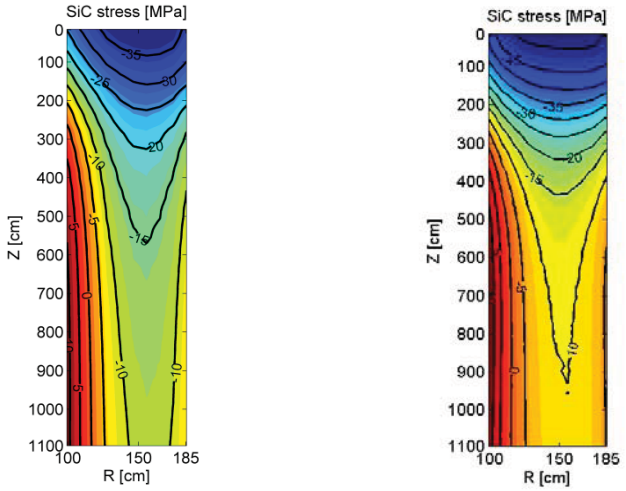

(a) (b)

Figure 35. SiC coating stress, for a pebble that has been (re)introduced in the core 6 times, as function of the position in the DB core at nominal conditions for the Pu-only (a) and the Pu+MA (b) fueled designs.

A-6.3 EFFECT OF VARIATION OF THE SiC AND CARBON BUFFER LAYER THICKNESS

The coatings and the kernel of TRISO-coated fuel particles vary slightly in size (thickness, diameter) depending of the fabrication process and quality control procedure of the process. A variation in the coating dimensions from the reference values has an effect on the particle performance. For example, a reduction of the buffer layer results in less room to accommodate the gaseous fission products and therefore an increase in the buffer pressure. This leads to higher stresses in the other coating layers and, as a consequence, a higher failure probability.

As a result of the non-linear behavior of the mechanical stresses during irradiation, the stress state and failure probability of the average coated particle, one which is manufactured the exact dimensions of the design specifications, is not necessarily equal to the average stress state of all the various particles, which show small deviations from exact specifications.

If the distributions $f(x_1),\ldots,f(x_n)$ of the variation of coating thicknesses $x_1,\ldots,x_n$ are known, the consequent expected stress state E can be calculated from the distribution functions and a stress function $\sigma(x_1,\ldots,x_n)$:

$$E[\sigma(x_1,\ldots,x_n)] = \int_{a_n}^{b_n}\ldots\int_{a_1}^{b_1}\sigma(x_1,\ldots,x_n)f(x_1)\ldots f(x_n)dx_1\ldots dx_n \quad (1)$$

Note that it is assumed that the probability density functions are independent. Similarly, the expected failure probability of all the various particles can be calculated by replacing the stress function $\sigma(x_1,\ldots,x_n)$ by the failure probability function $\psi\big(\sigma(x_1,\ldots,x_n)\big)$, which predicts the failure probability as a function of a given stress state. Using this function and rewriting Equation (1) as a summation over discrete points results in:

$$E[\psi\big(\sigma(x_1,\ldots,x_n)\big)] = \sum_{x_n}\ldots\sum_{x_1}\psi\big(\sigma(x_1,\ldots,x_n)\big)p(x_1)\ldots p(x_n) \quad (2)$$

The above integral is calculated in the PASTA code. The failure probability ($\psi(\sigma(x_1,\ldots,x_n))$) for given particle dimensions is calculated from the coating stresses. This probability is weighted with the probability of the particle having these dimensions ($p(x_1)\ldots p(x_n)$). By subdividing the domains of the coating thicknesses into discrete parts, then carrying out evaluation and summation of the probabilities, the expected failure fraction of all the particles combined ($E[\psi(\sigma(x_1,\ldots,x_n))]$) is obtained.

A PASTA calculation has been performed assuming Weibull distributions for the SiC and carbon buffer layer thickness (μ_{SiC}=45 μm, σ_{SiC}= 5 μm and $\mu_{C_{buf}}$ =90 μm, $\sigma_{C_{buf}}$ = 5 μm). The failure probability of the SiC layer as a function of the SiC and carbon buffer thickness has been calculated assuming either a time and temperature dependent function or a more conservative value of O/f = 0.4 for the free oxygen production.

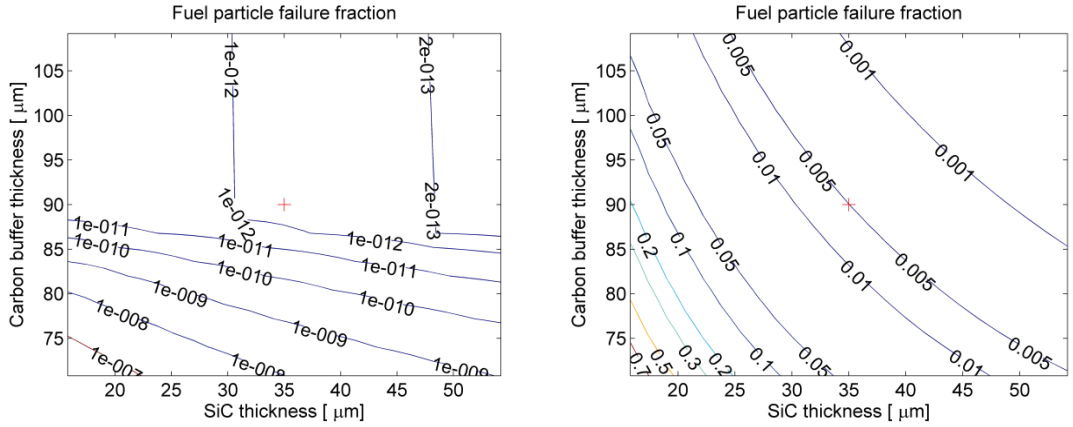

(a)[O/f (t,T)] (b)[O/f : 0.4]

Figure 36. SiC failure probability for the Pu-fueled DB core as a function of the buffer and SiC coating thickness assuming (a) O/f as a function of the irradiation time and temperature; and (b) for a fixed value of O/f =0.4 (b).

It can be seen that for O/f (t,T) the particle failure probability remains low for all coating dimensions with an overall failure probability of $3.8\cdot 10^{-11}$. However, if a more conservative value of O/f = 0.4 is assumed high failure probabilities can be expected with an overall value of $8.0\cdot 10^{-3}$.

A-7. TRANSIENT ANALYSIS OF THE FUEL PERFORMANCE DURING A LOSS OF FORCED COOLING INCIDENT

During a LOFC incident, the central part of the core can be expected to reach considerably higher temperatures than the nominal normal operation values. The pressure in the buffer layer is directly dependent on the temperature, but also indirectly through the diffusion of fission products and though CO production. Furthermore, the stress in the SiC layer is a function of the thermal expansion of the SiC layer itself and the PyC layers.

A LOFC transient calculation has been performed using a standalone thermal-hydraulics calculation in PEBBED. Figure 37 shows the core maximum fuel temperature history of a LOFC transient and core temperature profile at the time point of the maximum temperature (t = 47 h).

The stress calculation procedure for the transient is as follows:

1. For each point in the lifetime (irradiation dose and time) of the coated particle fuel, the stresses in the coatings are calculated assuming normal operation of the reactor. The histories of the fuel temperature, fission product build-up, irradiation time, and fast fluence (E > 0.1 MeV) during the lifetime of a pebble are generated with PEBBED by calculating the equilibrium core.
2. The fuel temperature history for each position in the core is generated by a DLOFC transient calculation in THERMIX. During this transient, the temperature difference between pebble surface and pebble center is small compared to normal operating reactor temperature differentials since heat production originates from decay heat only. Therefore, it is assumed that for a given location in the core, pebbles with a different burnup state (i.e., representing different points in the lifetime of the pebble) experience the same temperature history during the transient.
3. The temperature history of a pebble now consists of two parts. The first part represents normal reactor operation, in which the pebble reaches a given point in life at which the transient is initiated. At this point the pebble has passed several times through the core and has reached a certain core position. The second part of the pebble temperature history is determined by the temperature that this core location has during the transient (Figure 38).
4. For each position in the core the six possible temperature histories are used to calculate the corresponding histories for the pressure build-up in the buffer layer.
5. The stress state of the coatings is calculated during the entire lifetime (normal operation plus the transient part) of the pebbles (Figure 38).

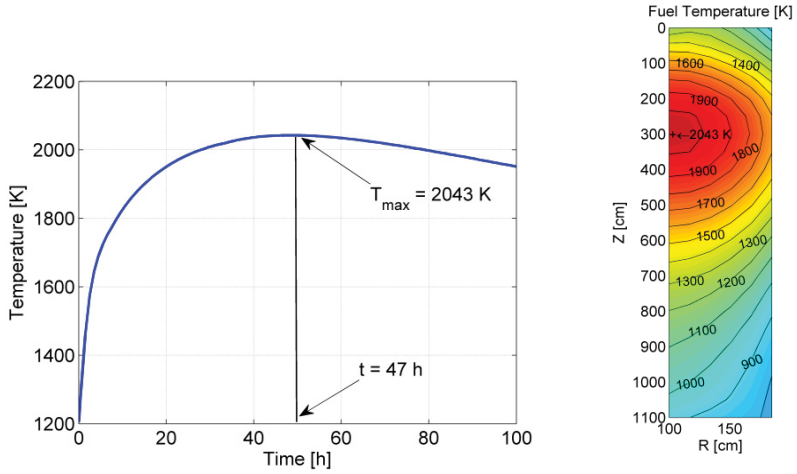

(a) (b)

Figure 37. (a) Core maximum fuel temperature history; and (b) the fuel temperature profile at the time the maximum temperature is reached.

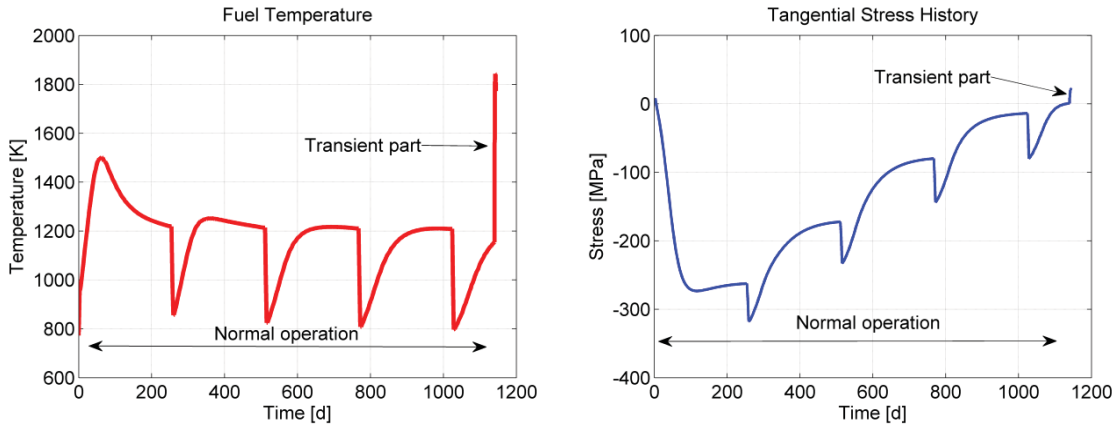

(a) (b)

Figure 38. (a)Temperature and (b)stress history for a pebble that has been (re)loaded in the core 5 times and is located in the top region of the core. The increase in temperature during the 100-hour-long LOFC transient results in an increase of the SiC stress.

The behavior of the buffer pressure and the resulting SiC stress during the transient for several axial core positions is shown in Figure 39. It can be seen that for some positions the buffer pressure and SiC stress significantly increase during the transient, which increases the failure probabilities of the particles in the respective core regions.

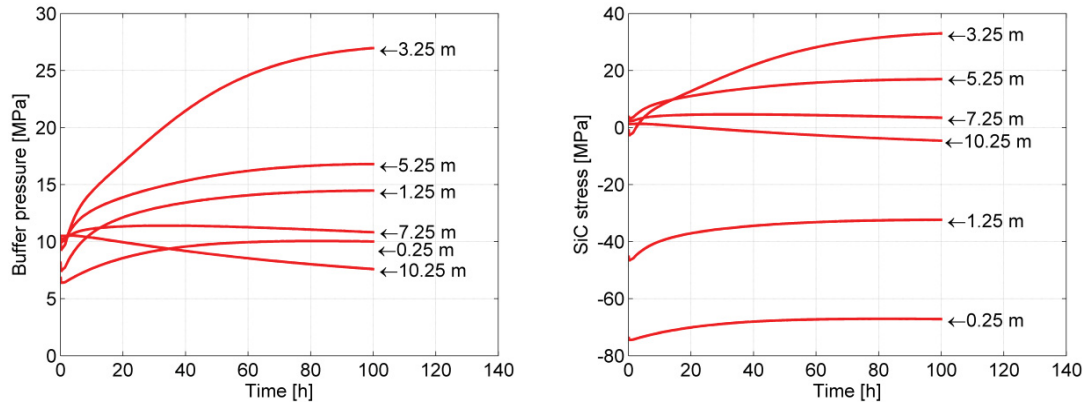

(a) (b)

Figure 39. (a) Pressure and (b) SiC stress history for several axial core positions during a DLOFC transient.

A-7.1 DB PEBBLE BED FUEL PERFORMANCE CONCLUSIONS

The fuel performance of DB fuel has been investigated using the improved PASTA-PEBBED code system for coated particle stress analysis. The predicted failure fractions for the different cases are presented in Table 15.

Table 15. Fuel failure probabilities.

Fuel type	Nominal conditions		LOFC transient
	O/f : (t,T)	O/f = 0.4	O/f : (t,T)
Pu	3.8×10^{-11}	8.0×10^{-3}	2.6×10^{-4}
Pu + MA	5.7×10^{-16}	1.9×10^{-3}	9.4×10^{-7}

It was found that the average (reference dimensions and average core radial temperature) fuel particle performs well. However, if a more conservative value for O/f is assumed, significant fuel failure can be expected, especially for LOFC conditions. To reduce failure probability, an improved fuel or core design is desirable for the DB pebble bed reactor.

A-8. INTER-COMPARISON OF FUEL PERFORMANCE CODES FUEL COATED PARTICLE STRESS ANALYSIS

In the framework of the DB project, several codes (PASTA, COPA, and PISA) have been used to analyze the durability of the coated particle fuel for various scenarios.

In lieu of a full-fledged and comprehensive Verification and Validation process, the PASTA [16], COPA [17], and PISA [18,19] codes have been used in a fuel performance comparison through collaboration between INL, General Atomics, and the Korea Atomic Energy Institute [20]. The comparison, which is meant to identify potential weaknesses of the various codes as well as build confidence in their respective performances, is presented in the following sections.

The codes employ different models and assumptions for the analysis of the coated particle performance. These differences can be found in the models for stress analysis on the various layers of the TRISO particle, models for fission products release, migration and accumulation within the TRISO particle, models for free oxygen and CO formation and migration, models for temperature field within the various layers of the TRISO particle, and models for the prediction of failure rates. Moreover, the possibility that different constitutive data for mechanical and thermal properties might be used implies a high likelihood for the three codes to give different results in the modeling of identical situations.

An inter-comparison has been carried out by the cooperating institutions within the workscope of the Department of Energy (DOE) Deep-Burn Project, using a common set of predefined TRISO conditions (burn-up levels, temperature or power levels, etc.). The coated particle under investigation is a design that is currently considered within the Deep-Burn Project to be fabricated within the near future. Besides the inter-comparison of the results for the codes prediction of performance for this fuel design, additional investigations are performed to quantify the sensitivity to input parameters. Finally, conclusions are drawn regarding both the performance analysis methods and the performance of the envisioned DB particle design.

A-8.1 DESCRIPTION OF THE DB COATED PARTICLE DESIGN USED FOR CODE-TO-CODE COMPARISON

The coated particle design specifications used for the inter-comparison are derived from the particle design that is considered for fabrication in the near future within the Deep-Burn Project. The fuel kernel consists of TRUs and a SiC getter that reduces the CO production in the particle. The mole ratio of TRU to SiC (TRU:SiC) in the kernel is 1:0.6, corresponding to an average density of 7.6 g/cm^3. The MA oxide (MAO2−x) fuel is sub-stoichiometric having on average 1.8 oxygen atoms per MA atom. The isotopic

compositions of the TRUs are shown in Table 16. Table 17 shows the dimensions of the kernel and coating layers and their statistical size variations.

Table 16. Isotopic composition of Deep-Burn fuel.

Isotope	Fraction (wt%)
Np-237	6.8
Pu-238	2.9
Pu-239	49.38
Pu-240	23
Pu-241	8.8
Pu-242	4.9
Am-241	2.8
Am-242m	0.02
Am-243	1.4

Table 17. Dimensions of the coating layers and their statistical variations for the selected DB coated particle design.

Layer	Thickness (μm)	Density (g/cm3)
Kernel ($MAO_{1.8}(SiC)_{0.6}$)	350*±10	7.6
Buffer	100±5	1.0
IPyC	35±5	1.9
SiC	45±5	3.2
OPyC	35±5	1.9

*Kernel diameter.

To make the comparison between the fuel performance codes possible, predefined boundary conditions (Table 18) are adopted rather than allowing the use of core physics analysis tools. It is assumed that the fuel particle has a fixed (outer surface) temperature of 1200 K at a power level of 2.0×10^{-2} W for 1120 days of irradiation in the core. The temperature within the kernel and in the coating layers is calculated by the fuel performance codes from the particle surface temperature and kernel power. At the end of the irradiation, the particle reaches a burn-up level of 560 MWd per kilogram of initial heavy metal (IHM) loading. The adopted parameters are taken from a PEBBED analysis of a Pebble Bed Modular Reactor design (400 MWth) loaded with DB fuel (Table 16) [21]. In the inter-comparison case, the fuel burn-up and the fast neutron fluence level attained are linear functions of the irradiation time since the kernel power level is assumed to be constant. It is noted that the boundary conditions presented above are intended to represent the typical environment of a DB reactor core without making any specific assumptions about the type of reactor (pebble bed or prismatic).

Table 18. Assumptions and boundary conditions adopted in the fuel performance analysis.

Final burn-up level	560 MWd/kg IHM
Final fast fluence (E > 0.1 MeV)	5.0×10^{21} cm^{-2}
Particle surface temperature	1200 K
Kernel power	2.0×10^{-2} W
Irradiation time	1120 days

In the following section (Section A-8.2), the results of the fuel performance analysis from the three codes are compared and analyzed. In Section A-8.3 the sensitivity of the results on several input parameters is investigated.

A-8.2 ANALYSIS OF THE REFERENCE COATED PARTICLE

During the irradiation of the coated particle fuel, gaseous fission products that are formed in the kernel that diffuse to the porous carbon buffer layer. Figure 40 shows the amount of fission products released from the kernel to the buffer layer as a function of the fast neutron fluence attained. The PASTA and COPA codes assume the release occurs according to the Kidson and Booth models [22], in which diffusion of the fission products is a function of time and temperature; PISA assumes a fixed value of 60% release fraction. As a result, the PISA code gives a linear build-up of the fission products in the buffer layer, while in the PASTA and COPA codes the release is somewhat delayed (Figure 41). It is noted that no formation of CO by free oxygen is expected, since the kernel contains a SiC getter. Furthermore, the contribution of He is assumed to be negligible.

The computed results for the available (void) volume for the gaseous fission products are shown in Figure 42. In the PASTA and PISA codes the initial void volume in the buffer is calculated according to:

$$V_{void} = 1 - \frac{\rho_{buf}}{\rho_{graphite}} \tag{3}$$

in which, ρ_{buf} is the buffer density and $\rho_{graphite}$ is the theoretical maximum value of the density of graphite. The COPA code assumes that the kernel volume also has some void space (0.5% of the kernel pore volume). Furthermore, the PISA and COPA codes assume that the void space in the buffer decreases with increasing radiation due to kernel swelling, which is caused by build-up of solid and gaseous fission products.

The build-up of gaseous fission products in the buffer causes a pressure rise (Figure 43) on the IPyC layer, which is calculated by all three codes by the Redlich-Kwong equation of state. The pressure is directly dependent on the buffer void volume. Therefore the PISA code calculates the highest pressure and the PASTA code the lowest, resulting from the low and high values for the void volume, respectively.

In principle, the buffer pressure results in a tangential tensile stress on the SiC layer, which is the main load-bearer of the particle. However, the PyC layers shrink (Figure 44) and thereby put the SiC under compression. The following references and assumptions were used by the codes to determine the PyC dimensional change as a function of the fast fluence level:

- COPA: Reference [23], with ρ_{PyC} = 1.9 g/cm^3 , T = 1200 K, BAF_0=1.0
- PASTA: Reference [23], with ρ_{PyC} = 1.9 g/cm^3 , T = 1200 K, BAF_0=1.036
- PISA: Reference [24] page 30, with T = 1473 K, BAF_0=1.036.

In the above, BAF stands for the Bacon Anisotropy Factor, a measure of the degree to which pyrolytic carbon (or graphite) departs from an isotropic structure.[25] The shrinkage and swelling behavior of the PyC layers is a function of the BAF, which is determined by the fabrication process of the layers. For a PyC layer that is isotropic (BAF = 1), the dimensional change in the radial and tangential dimensions are equal, which is assumed in the COPA code. The PASTA and PISA codes assumed that the PyC is slightly anisotropic (BAF = 1.036), which results in less shrinkage of the PyC in the radial direction in the early stages of irradiation. Furthermore, there exists a turnaround point where the shrinkage in the radial direction turns to swelling. It is noted that the effective length of the PyC layers in the tangential direction is significantly larger than in the radial one, which makes the dimensional change behavior of the first, the more important.

At the beginning of irradiation of the particle, the dimensional change of the PyC layers determines the stress state of all three layers (IPyC, SiC, and OPyC) entirely (Figure 45–Figure 47). Since the three codes use similar dimensional change rates of the PyC in the tangential direction there is good agreement between the codes for the calculated stresses for low fluence levels. With increasing fluence some differences can be identified, which can be explained as follows. The PASTA code has a lower buffer pressure than the COPA code, resulting in lower stress on the SiC layer at the end of the irradiation. The PISA code has a higher buffer pressure than PASTA, but this seems to be compensated by the higher shrinkage (tangential) rate of the PyC. Therefore the PASTA and PISA codes show a similar result for the final SiC stress at the end of the irradiation.

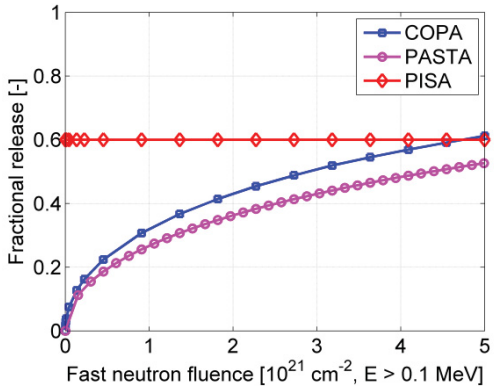

Figure 40. Fractional release of gaseous fission products from the fuel kernel to the buffer layer, calculated by the COPA, PASTA, and PISA codes.

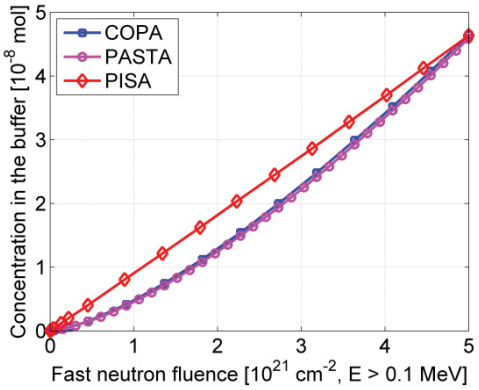

Figure 41. Concentration of Xe and Kr in the buffer layer calculated by the COPA, PASTA, and PISA codes.

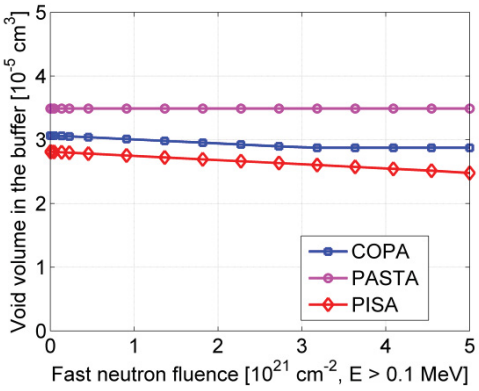

Figure 42. Void volume in the buffer layer calculated by the COPA, PASTA, and PISA codes.

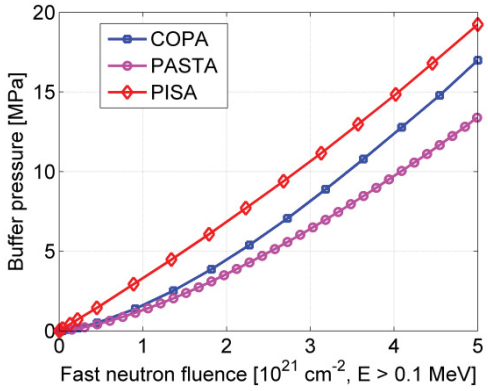

Figure 43. Buffer pressure calculated by the COPA, PASTA, and PISA codes.

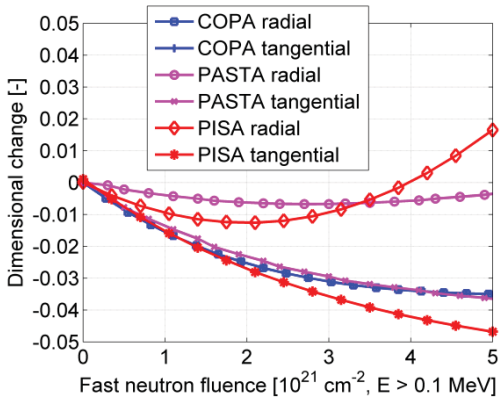

Figure 44. Correlations for the PyC dimensional change

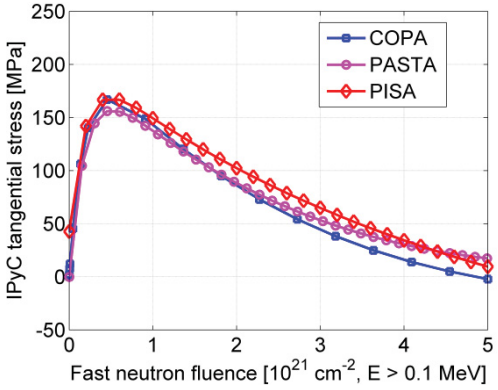

Figure 45. Tangential stress in the IPyC layer calculated by the COPA, PASTA, and PISA codes.

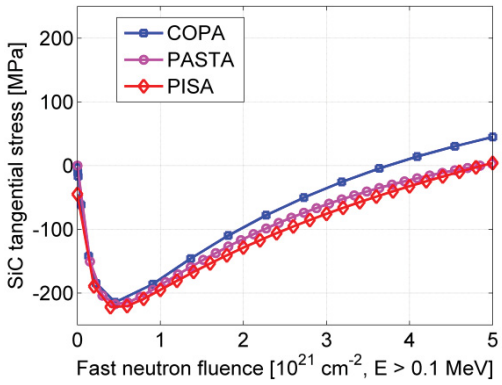

Figure 46. Tangential stress in the SiC layer calculated by the COPA, PASTA, and PISA codes.

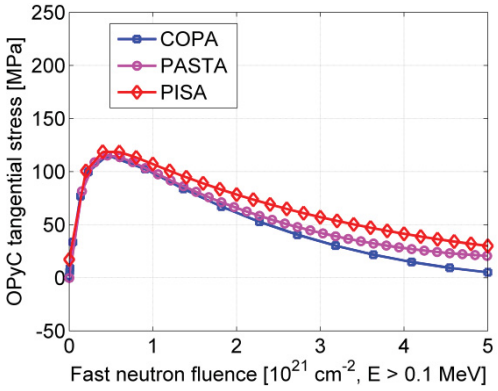

Figure 47. Tangential stress in the SiC layer calculated by the COPA, PASTA, and PISA codes.

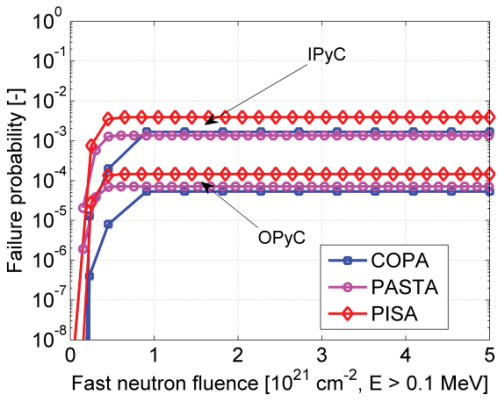

Figure 48. Cumulative failure probability of the IPyC and OPyC coating layers as a function of the fast fluence calculated by the COPA, PASTA, and PISA codes.

There is a relatively good agreement between the failure probabilities predicted by the three codes (Figure 48), because the maximum IPyC and OPyC stresses are similar. Although the failure probability of the IPyC layer is relatively high, no significant failure probability was found for the SiC layer. While the PASTA and PISA codes calculate the failure probabilities directly from the stress levels, the COPA code performs a Monte-Carlo calculation to determine the failure probability.

A-8.3 SENSITIVITY OF INPUT PARAMETERS ON FUEL PERFORMANCE

In the previous section some differences in the findings were identified that result from the various assumptions made in the codes. Specifically, the buffer void volume and the dimensional change of the PyC layers are modeled differently, which leads to a small spread in the predicted coating stresses and failure probabilities. Additional studies have to be carried out in order to quantify the coating stress and failure probability of the layers sensitivity to several input parameters. Sensitivity to the following parameters has been investigated:

- The available volume (void) for the fission products in the buffer and kernel
- The particle coating dimensions
- The dimensional change of the PyC layers
- The creep coefficient of the PyC layers.

The effect of the variation in the thickness of the SiC and buffer layers has been investigated with the PASTA code. The two layers were allowed to vary around their respective average values, assuming a normal distribution with a standard deviation of 5 μm, as in Table 17. The failure probability for a given set of coating dimensions was weighted with its probability of occurrence. It was found that the variation in coating size did not have a large impact on the average failure probability of the SiC layer.

The failure probability of this batch of particles was found to be $<1\times 10^{-9}$.

An analysis was carried out with the PASTA code using three different BAF values, which translate into three different PyC irradiation-induced dimensional change rates for the radial and tangential directions (Figure 49). It can be seen from Figure 50 that the final stress level of the SiC layer is especially sensitive to the dimensional change of the PyC, while the maximum stress of the IPyC or OPyC is relatively

insensitive. This conclusion appears to be at variance with observations during irradiations and with the importance usually assigned to the BAF of pyrocarbon coatings.

From the analysis in the previous section it was found that the maximum stress in the PyC layers (170 MPa) is relatively close to its median strength (300 MPa). This is expected to be the result of a relatively low value of the creep coefficient for radiation induced creep. An additional case was investigated with the PISA code in which the creep coefficient was doubled. The results for the coating stresses are shown in Figure 51. It can be seen that the increased creep coefficient reduces the effect of the dimensional change of the PyC layers. The tangential stresses are lower in all three layers for the increased creep coefficient case, while the SiC stress at the end of the irradiation is higher.

The PASTA code has been used to investigate the sensitivity of the void volume in the buffer on the SiC stress. Results are shown in Figure 52. It can be seen that a reduction of the void volume significantly increases the SiC, while an increase of the void volume only results in a moderate reduction of the stress.

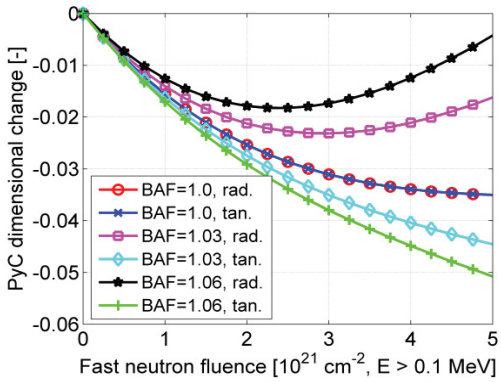

Figure 49. Irradiation induced dimensional change as a function of the fast fluence level (E > 0.1 MeV) for three BAF values (1.00, 1.03, 1.06).

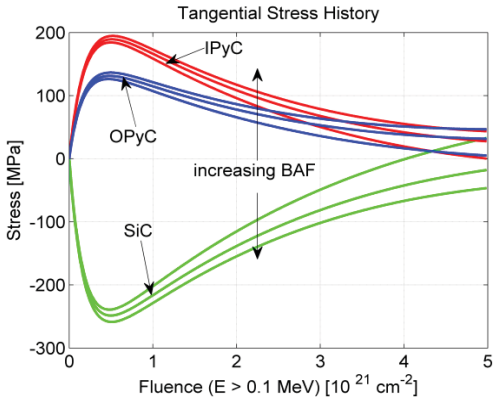

Figure 50. Effect of the BAF value (1.00, 1.03, 1.06) on the stresses in the coating layers (IPyC, SiC, OPyC) during irradiation.

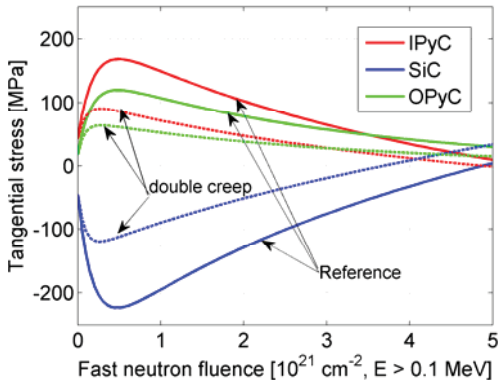

Figure 51. Tangential stress as a function of the fast fluence calculated by the PISA code, assuming either the reference value for the creep coefficient (2.0×10^{-29}(MPa.m^{-2})$^{-1}$) or double this value.

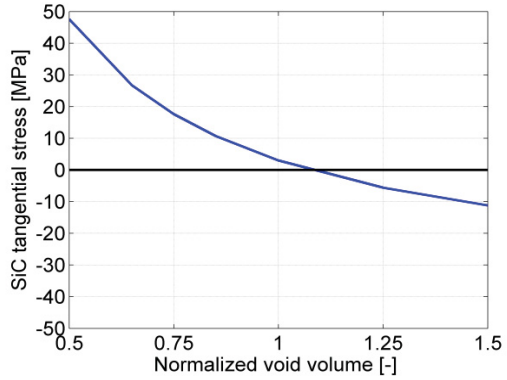

Figure 52. The maximum stress in the SiC layer during the irradiation as a function of the void volume in the buffer calculated with the PASTA code (reference volume = 3.5 × 10−6 cm^3).

A-8.4 CONCLUSIONS REGARDING FUEL PERFORMANCE MODELING OF DEEP-BURN COATED PARTICLES

An inter-comparison of the fuel performance modeling of DB-coated particle fuel has been performed. It was found that there are several differences in the modeling approach between the COPA, PASTA, and PISA codes.

- The models for the void volume in the kernel and buffer layer to which the fission products diffuse differ slightly between the codes. In the PISA and COPA models, the kernel is assumed to expand as a function of the irradiation level, thereby reducing the buffer void volume. Therefore, the buffer pressure in these models is higher, which results in a higher SiC stress.
- The dimensional change of the PyC layers has a large impact on the stress state of the coating layers. For a coated particle design that has a sufficient buffer volume to accommodate the fission products, the dimensional change determines the stress state of the coatings almost entirely.
- The effect of the dimensional change of the PyC layer is reduced in cases when the layers exhibit significant radiation induced creep. Proper experimental data on PyC radiation induced strain creep are essential to the accurate prediction of coated particle performance.

A-9. PRELIMINARY ANALYSIS OF AN EARTHQUAKE EVENT FOR DEEP BURN PBR (S. Sen and A. M. Ougouag)

The safe shutdown earthquake with passive mode core conduction cooling to the Reactor Cavity cooling system was identified as one of the design basis accidents (DBA) for the South African pebble bed reactor PBMR. A similar event was identified as a DBA for the Chinese experimental pebble reactor HTR-10. The regular NGNP-type pebble bed reactor was shown previously to shut down passively to a safe state in the event of an earthquake. This section describes briefly the behavior of a reactor fueled with DB fuel. For this work the standard INL codes for analysis of pebble reactors have been used, although some aspects of said codes still need further development and refining in order to produce fully reliable results. Nonetheless, a preliminary study has been carried out and the results presented here are meant as an indication of expected trends and not meant to be a definitive statement on the subject.

The tools that were used for this work are the

- CYNOD code [26]: this code uses a cylindrical geometry finite difference or nodal neutron diffusion method to solve for the neutron flux (and hence power) in pebble bed transients. The code is coupled with THERMIX-KONVEK code [27], which provides it with thermal-hydraulics feedback and is augmented with a TRISO-level heat transfer model embodied in the THETRIS code 28, which is necessary for the correct treatment of the Doppler effect.
- COMBINE [29] is used for generation of multigroup diffusion data. The code is used iteratively with CYNOD as described below.
- PEBBLES [30] is used once to generate the packing pattern of the pebbles in the pebble bed and then to simulate the shaking during an earthquake and generate time-dependent pebble distributions. The data generated by PEBBLES are post-processed using the utility code SHAKE [28] in order to translate the pebbles packing pattern into approximate fuel densities and recomputed cross sections and diffusion coefficients.

In the course of this work the CYNOD code was modified to account for leakage effects on macroscopic multigroup nuclear data. The code is now implemented as part of a new scheme that is shown in Figure 53.

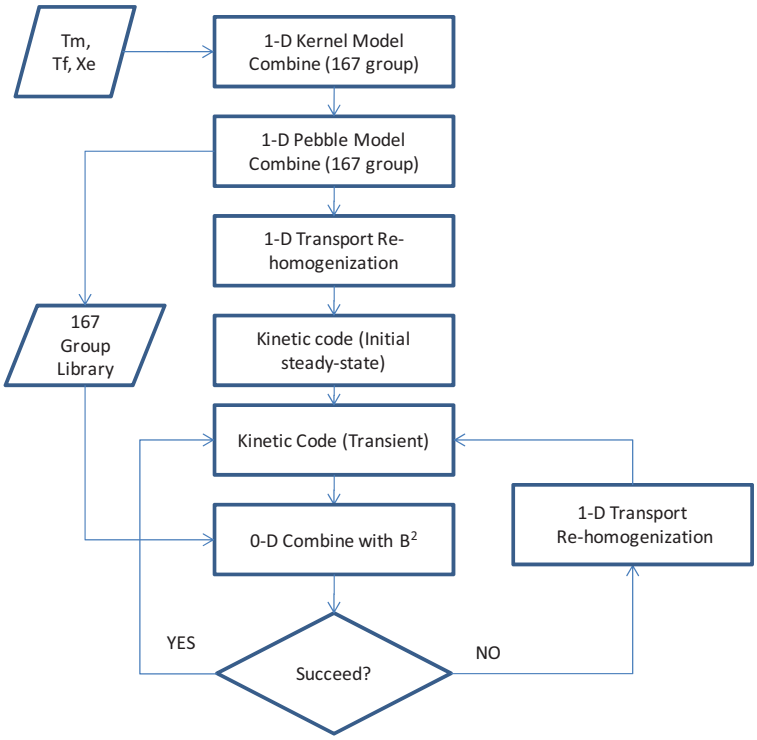

Figure 53. CYNOD kinetic computational scheme with embedded cross section generation

CYNOD requires few-group tabulated macroscopic cross sections and diffusion coefficients prior to the analysis. The macroscopic cross sections are generated for a given deep-burn pebble bed reactor using PUMA fuel with 2.0 g HM loading per pebble. The PUMA fuel is nearly identical to the DB fuel. The study was not repeated with optimized DB fuel.

The flow chart of Figure 53 extends to kinetic applications a previously developed scheme adapted to steady-state and depletion [31]. The new feature in this flowchart is that the spectral correction introduced in [31] is applied because of changes in the spectrum caused by the transient rather than changes caused by depletion. In the present application, the correction is needed more frequently than in depletion, but the principle remains the same. The features of the chart are self explanatory. The first box refers to an infinite cell calculation at the TRISO and associated matrix level (with Dancoff correction); the second box does the same for a pebble-level cell. The third box is a 1-D transport re-homogenization step in which the spectral effects from the reflectors are captured prior to the homogenization and collapsing in energy group structure to a few groups.

During the course of a transient, conditions change and induce changes in the spectrum (e.g., because of temperature changes and hardening of the spectrum or control rod insertion and softening or other artifacts). At that point, using leakage data from the full core spatial solution a buckling is estimated and then supplied to the COMBINE code for the performance of a point (or zero-D) re-estimation of the

spectrum and re-collapsing of the data spectral zone by spectral zone. At the conclusion of this step if the new data are deemed satisfactory the next kinetic step is carried out, if not, a full-fledged transport re-homogenization step is carried out before the next kinetic step is taken. In this way the spectrum-induced error in the cross sections is controlled continuously throughout the simulation.

An earthquake causes the pebbles in a pebble bed reactor to density as they become overall better packed (just like packing fraction increases when a jar of sugar is shaken to make room for more sugar). The packing of the pebbles induces a reactivity insertion because of the higher fuel density. In addition, if the control rods are not intentionally moved, there results an effective relative withdrawal of the rods, which also inserts reactivity. Assuming no SCRAM, the only safety mechanism for countering these reactivity insertions is the Doppler Effect. Figure 54 shows the response of the model reactor considered here to the INL site design basis earthquake. The figure amply demonstrates that the reactor shuts down with a sharp drop in power and a relatively slow and moderate increase in temperature. The results displayed in the figure stop after forty seconds of simulation. However, after that time, the dynamic of the reactor is driven by decay heat only, and the models presented in other parts of this report show that most design under consideration here do not lead to adverse effects under shut down conditions with decay heat as the only source of energy into the core. Of course, some time after the shut down (i.e., after the earthquake) control rods will have to be inserted, as the temperature would start to decrease and re-criticality might occur. For a previously long-operated reactor the concern may not arise until after the Xenon that builds up after shut down has finally decayed to levels that allow re-criticality.

The principal conclusion of this preliminary study is that the DB-like reactor considered here would passively shut itself down in the event of an earthquake and would be in a status that remains safe until further action can be taken and such actions would not be immediately required.

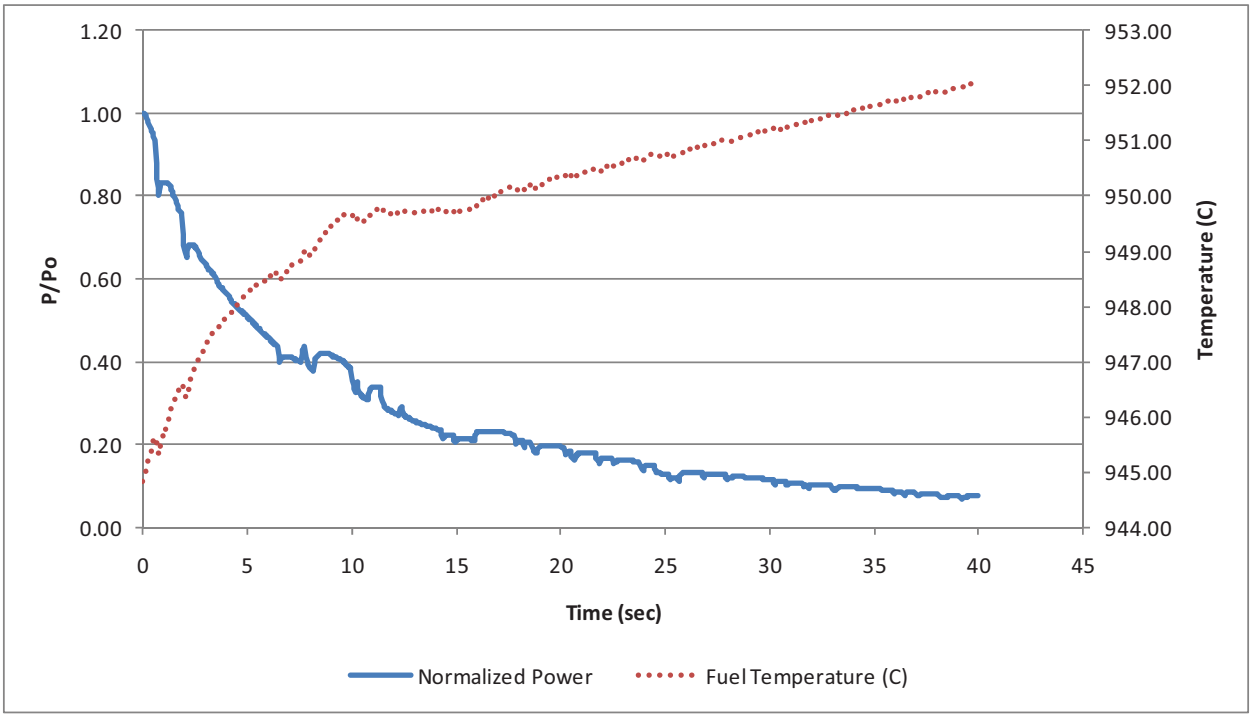

Figure 54. Neutronic and thermal-hydraulic (power and temperature) response of a DB-like pebble bed reactor to earthquake-induced reactivity insertion and no SCRAM

REFERENCES

[1] Versluis, R. M., Venneri, F., Petti, D., Snead, L., and McEachern, D., 2008, "Project Deep-Burn: Development of Transuranic fuel for High-Temperature Helium-Cooled Reactors," *Proc. of the 4th International Topical Meeting on High Temperature Reactor Technology (HTR2008), Washington DC, USA, 2008*.

[2] Reitsma, F., 2004, "The Pebble Bed Modular Reactor Layout and Neutronics Design of the Equilibrium Cycle," *In Proceedings of PHYSOR-2004, Chicago, USA, April 25-29, 2004*.

[3] Lohnert, G.H., 1990, "Technical design features and essential safety-related properties of the HTR-MODULE", *Nuclear Engineering and Design*, **121,** p. 259-275.

[4] de Haas, J.B.M, and Kuijper, J.C., 2005, "Feasibility of burning first- and second-generation Plutonium in pebble bed high-temperature reactors", *Nuclear Technology,* **151**, p. 192-200.

[5] Zheng, Y., Shi, L. and Dong, Y., 2009, "Thermohydraulic transient studies of the Chinese 200 MWe HTR-PM for loss of forced cooling accidents", *Annals of Nuclear Energy,* **36,** p. 742-751.

[6] Terry, W. K., Gougar, H. D., and Ougouag, A. M., 2002, "Direct Deterministic Method for Neutronics Analysis and Computation of Asymptotic Burnup Distribution in a Recirculating Pebble-Bed Reactor," *Annals of Nuclear Energy*, **29**, p. 1345–1364, 2002.

[7] ORNL, 2009, *SCALE-6: A Modular Code System for Performing Standardized Computer Analyses for Licensing Evaluations*, ORNL/TM2005/39, Version 6.0, Vols I-III, ORNL, 2009.

[8] Teuchert, E., et al, 1994, "V.S.O.P. – Computer Code System for Reactor Physics and Fuel Cycle Simulation," Forschungszentrum Jülich GmbH Jül-2897, 1994.

[9] Goluoglu, S., 2006, "Analysis of a Computational Benchmark for a High-Temperature Reactor Using SCALE," *Proceedings of PHYSOR 2006*, *Vancouver, BC, Canada, September 10–14, 2006*.

[10] OECD/NEA, 1999, "Status and Assessment report on Actinide and Fission Product Partitioning and Transmutation".

[11] ICRP, 1996, ICRP Publication 72: "Age-dependent Doses to the Members of the Public from Intake of Radionuclides", Part 5, Compilation of Ingestion and Inhalation Coefficients, *Annals of the International Commission on Radiological Protection*, **26**:1.

[12] Tucek, K. "Neutronic and Burnup studies of Accelerator-driven Systems Dedicated to Nuclear Waste Transmutation", PhD thesis (KTH), Stockholm 2004.

[13] Zheng, Y., L. Shi, and Y. Dong, 2009, "Thermohydraulic transient studies of the Chinese 200 MWe HTR-PM for loss of forced cooling accidents," *Annals of Nuclear Energy*, **36**, 742–751, 2009.

[14] Zhang, Z., Z. Wu, D. Wang, Y. Xu, Y. Sun, F. Li, Y. Dong, 2009, "Current status and technical description of Chinese 2x 250 MW_{th} HTR-PM demonstration plant," *Nuclear Engineering and Design*, **239**: 1212–1219, 2009.

[15] Kugeler, K., and R. Schulten, *Hochtemperaturreaktortechnik*, Springer-Verlag, 1989.

[16] Boer, B., A. M. Ougouag, J. L. Kloosterman, and G. K. Miller, 2008, "Stress analysis of coated particle fuel in graphite of High-Temperature Reactors," *Nuclear Technology*, **162**, p. 276–292, 2008.

[17] Kim, Y. M., M. S. Cho, Y. W. Lee, W. J. Lee., 2008, "Development of a Fuel Performance Analysis Code COPA," *In Proceedings of the 4th International Topical Meeting on High Temperature Reactor Technology (HTR-2008). Washington D.C., USA, September–October 2008*.

[18] CEGA-002549, 1993, "PISA -Software Requirement Specifications for Code to Perform Mechanical Analysis of Irradiated Fuel Particles," Technical report, CEGA Corporation, 1993.

[19] CEGA-002550, 1993, *PISA: A Coupled Thermal-Stress Code for the Mechanical Analysis of Irradiated Fuel Particles* – User's Manual, Technical report, CEGA Corporation, 1993.

[20] Boer, B., Y. M. Kim, W. Wu, A. M. Ougouag, D. McEachern, F. Venneri, 2010, "Inter-comparison of Computer Codes for TRISO-based Fuel Micro-Modeling and Performance Assessment," *Proceedings of HTR 2010, Prague, Czech Republic, October 2010*.

[21] Boer, B., A. M. Ougouag, 2010, "Core Analysis, Design and Optimization of a Deep-Burn Pebble Bed Reactor." *In Proceedings of the PHYSOR 2010 -Advances in Reactor Physics to Power the Nuclear Renaissance. American Nuclear Society, Pittsburgh, USA, May 2010*.

[22] G. Kidson. "A generalized analysis of the cumulative diffusional release of fission product gases from an equivalent sphere of UO_2," *Journal of Nuclear Materials*, **88**, p. 299–308, 1980.

[23] Ho, F., 1993, "Material Models of Pyrocarbon and Pyrolytic Silicon Carbide," Technical Report CEGA-002820, CEGA Corporation, San Diego, CA, 1993.

[24] INERI, 2004, "Development of improved models and designs for coated-particle gas reactor fuels." Technical Report INEL/EXT-05-02615, Final report under the international nuclear energy research initiative, December 2004.

[25] Bacon, G. E., *J. Appl. Chem.*, **6**, 477 (1956).

[26] Hiruta, H., Ougouag, A., Gougar, HD, "CYNOD Version 2.0a Input Manual", INL, August, 2008

[27] Teuchert, E., et al., 1994, V.S.O.P. ('94) Computer Code System for Reactor Physics and Fuel Cycle Simulation - Input Manual and Comments, April 1994.

[28] Ortensi, J., "An Earthquake Transient Method for Pebble-Bed Reactors and a Fuel Temperature Model for TRISO Fueled Reactors", PhD Thesis, Idaho state University, Sept. 2009

[29] Yoon, WY, Grimesey, RA, Nigg, DW, Curtis, RL, "COMBINE7.1-A portable ENDF/B-VII.0 Based Neutron Spectrum and Cross-Section Generation Program", INL/EXT-08-14729, Rev 1, August, 2009

[30] J. J. Cogliati, A. M. Ougouag, "Pebbles: A Computer Code for Modeling Packing, Flow and Re-Circulation Of Pebbles In A Pebble Bed Reactor" High Temp. Reactor Tech. Johannesburg, South Africa, October 1-4, C00000180. (2006)

[31] N. H. Hudson et al. "A Pebble Bed Reactor cross section methodology" *Annals of Nuclear Energy*, **36** (2009) 1138-1150.